Electromagnetic Resonances of Cylinders and Aircraft Model with Resistive Wires

by
G. W. Wood
T. F. Trost

Report on
N.A.S.A. Grant NAG-1-28

November 1984

Department of Electrical Engineering
Texas Tech University
Lubbock, Texas 79409

ELECTROMAGNETIC RESONANCES OF CYLINDERS AND AIRCRAFT MODEL WITH RESISTIVE WIRES

by

G. W. Wood
T. F. Trost

Department of Electrical Engineering
Texas Tech University
Lubbock, Texas 79409

November 1984

Prepared for
National Aeronautics and Space Administration
Langley Research Center
Hampton, Virginia 23665

Under Grant No. NAG-1-28
"Lightning Sensors and Data Interpretation"

ABSTRACT

Laboratory experiments were done to determine the natural frequencies of the electromagnetic resonances of conducting bodies with attached wires. The bodies include two cylinders and an approximate scale model of the NASA F-106B aircraft. All are three feet in length. Time-domain waveforms of B-dot and D-dot are obtained from a sampling oscilloscope, and Prony analysis is used to extract the natural frequencies. This work is an extension of previous work, but smaller, more resistive wires have been used.

The first four natural frequencies of the cylinders (and wires) were determined, and a comparison with calculated results of other investigators shows reasonable agreement.

Seven natural frequencies were determined for the F-106B model (with wires), and these have been compared with results obtained by NASA in 1982 during direct lightning strikes to the aircraft. The agreement between the corresponding natural frequencies of the model and the aircraft is fairly good and is better than that obtained in the previous work using wires with less resistance. The frequencies lie between 6.5 MHz and 41 MHz, and all of the normalized damping rates are between 0.14 and 0.27.

This work was performed under NASA grant No. NAG1-28 with support from the Air Force Weapons Laboratory.

TABLE OF CONTENTS

LIST OF FIGURES

LIST OF TABLES

I. INTRODUCTION

The work described in this report represents one phase of an experimental study of the electromagnetic resonances of conducting bodies with attached wires. This work is similar to a previous investigation described in NASA CR 169455 [Ref. 1]; the major difference in the present case is the use of smaller, more resistive wires. The conducting bodies included two cylinders and an approximate scale model of an F-106B aircraft. The results from the cylinders have been compared with theoretical calculations to check the accuracy of this technique. The results from the aircraft model find application in the study of lightning strikes to airplanes. The wires represent, in an approximate sense, the lightning channel. Our results have been compared with those obtained from the NASA F-106B during direct lightning strikes. The need to interpret the data from the F-106B is the main motivation for the work reported here.

Section II of the report describes the laboratory technique employed to investigate the resonances. Short pulses of current were applied to the body under test through one of the attached wires, and free-field electromagnetic sensors or probes were used to measure the B-dot ($\partial B/\partial t$) and D-dot ($\partial D/\partial t$) fields as a function of time near the surface of the body. Two wires were used, one for current entry and the other for current exit. They were connected axially to the ends of the cylinders and to the nose and tail of the F-106B model, with the current input on the nose wire.*

A curve-fitting technique known as Prony analysis [Refs. 1,2,3,4] was used to study the resonances. The Prony code was run on the measured data and sets of poles and residues were extracted. Some of the poles could be interpreted as the natural frequencies of the body-and-wire system. Fourier analysis was also used on the data as an alternate approach for obtaining information on the resonances.

---

* In the previous investigation, sensors were mounted directly to the body, with an output cable inside one of the attached wires.

The Prony results for the cylinders are given in Section III. They show the expected weaker damping of the resonances for the resistive-wire case, and they are in agreement with theoretical calculations [Refs. 5,6].

The Prony results from the aircraft model are given in Section IV and compared with results obtained on the NASA F-106B [Ref. 7]. The comparison shows that the use of resistive wires brings the resonances of the model into better agreement with those observed in flight.

The results are summarized and conclusions drawn in Section V.

II. EXPERIMENTAL SETUP AND MEASUREMENT TECHNIQUE

Experimental Setup

A diagram of the experimental setup is shown in Figure 1. It consists of a pulse generator (Tektronix, Type 109), a 12-ft by 12-ft ground plane, a sampling oscilloscope with the appropriate plug-ins (Tektronix Type 568 Oscilloscope, Type 3S2 Sampling Unit, Type 3T2 Random Sampling Sweep Plug-ins, and Type S4 Sampling Heads), a monitor oscilloscope (Tektronix Type 7313), some in-house-built buffer amplifiers, and a computer with floppy disk drive for the digitizing and recording of waveforms (DEC PDP 11/04, Plessey PM-XS11). In the experiment, the object undergoing testing is either a cylinder or an F-106B model located 10 ft* above the ground plane, and attached to the rest of the experiment with wires having a resistance of 8.0 Ω to the foot and a diameter of 0.01 in.**

A roughly rectangular pulse with a 1.2-ns-wide base and a rise time and a fall time of 0.25 ns each, is applied at the ground plane. The pulse propagates up the lower wire, over the object under test, on up another resistive wire attached to the top of the test object, and from this wire to a low resistance wire attached to the ground. The EM field near the test object is measured with free-field sensors. The time required for a portion of the pulse to be reflected from the nose of the test object down to the ground plane and back up again is 20 ns. This gives a data window 20 ns wide in which to sample the waveform before it is corrupted by reflections.

Data Acquisition System

The acquisition of data from the probes is done by a computer specially modified for this task with a programmable clock to control the rate at which the computer samples the output from the sampling oscilloscope and an analog-to-digital converter which digitizes it. The A/D converter and the programmable clock are both standard commercially

---

* To convert feet to meters, multiply by 3.048 000 E-01.
** To convert inches to meters, multiply by 2.5400 000 E-02.

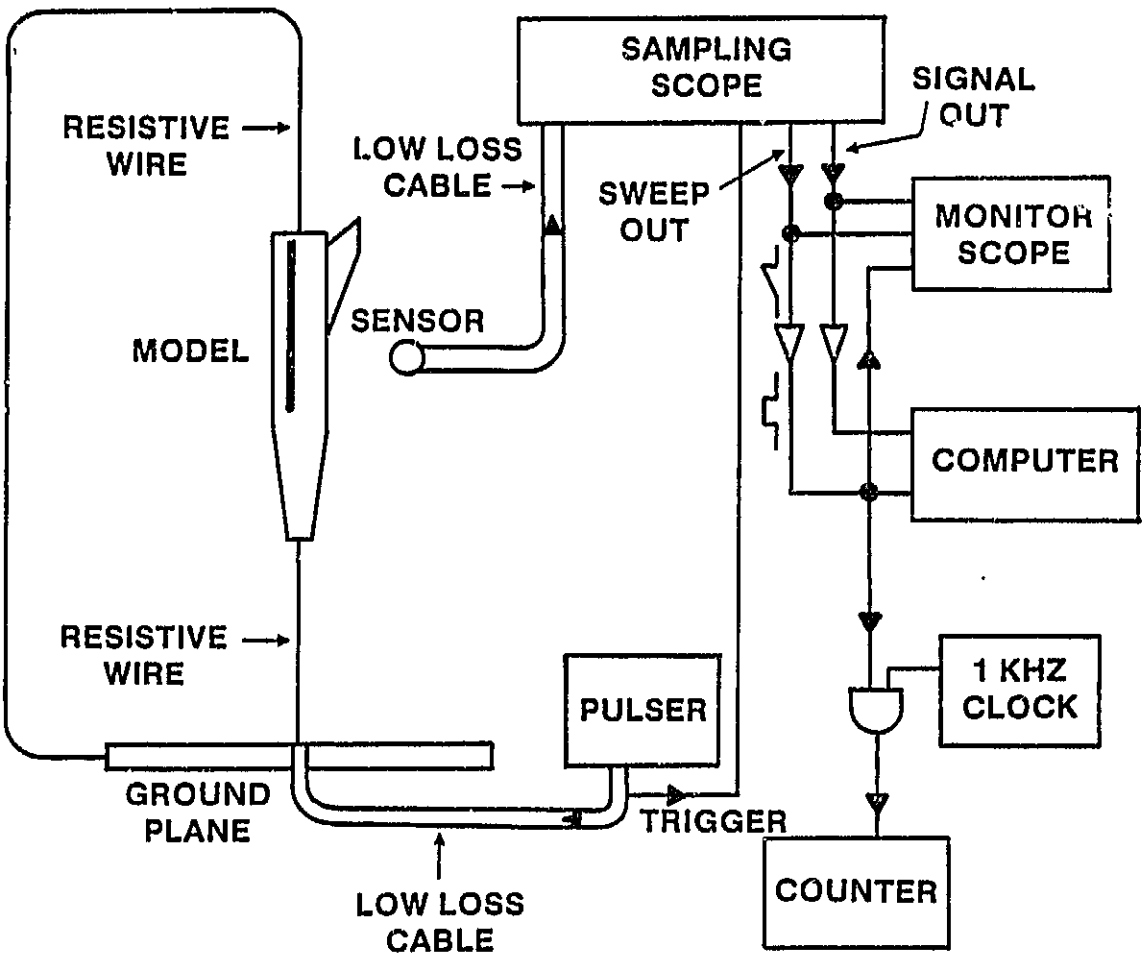

Figure 1. Diagram of experimental setup.

available boards which plug into the Q-bus of the PDP 11 series computer. The A/D converter is a Data Translation DT 1712. This board has a single 12-bit converter with 8 differential input channels multiplexed into it. The differential inputs are advantageous because the probes have two outputs, and it is the difference between the outputs that is of interest. The input range of the converter is from -10 V to +10 V; this makes one least significant bit equal to 4.88 mV. The maximum throughput rate is 35 kHz. The A/D board needs an external trigger to mark the start of the waveform to be converted. This signal is supplied by the programmable clock, a DEC KW11-K.

The external trigger used on the clock board is the "data window" signal. A "data window" is generated by using the horizontal sweep of the sampling oscilloscope to saturate a simple single 2N2222 transistor amplifier. The output of the saturated amplifier is essentially an asymmetric squarewave that is then used to accomplish three different tasks. The first is triggering the programmable clock in the computer. The second task is "windowing" the data that the computer is "seeing." The horizontal sweep for the monitor scope comes from the sampling oscilloscope, so that the two oscilloscopes have exactly the same sweep rate and the traces are synchronized. The third task is gating a counter to measure the length of time it takes for the sampling oscilloscope to complete a sweep.

The display on a sampling oscilloscope is the result of many repetitive pulses. Thus the actual sweep rate is much slower than the equivalent rate. Both rates must be accurately known. The equivalent sweep rate on both the sampling and the monitor oscilloscopes is equal to 2 ns per division, and there are 10 divisions on the graticules of both oscilloscopes. This corresponds to the 20 ns of clear time on the experiment. Due to the limited memory available in the computer, one can take only 400 samples off one sweep. Taking 400 samples in a 20 ns period gives an equivalent sampling period of 50 ps and a Nyquist frequency of 10 GHz. As will be shown later, this sampling rate is sufficient to prevent aliasing. The actual sampling rate is much lower. Roughly 1.98 s are required to complete a sweep or generate a waveform

for the computer to digitize. Taking 400 samples in this period of time yields an actual sampling rate of 206 samples/second.

The outputs from the sampling oscilloscope have an impedance of 10 kΩ, which can cause a problem with the multiplexer. If the cables to the multiplexer have too much capacitance, there is an undesirable "charge-up" time. There are two ways to correct this problem. The first is to use short cables, but there is a limit to how much capacitance can be removed this way. The second way is to lower the impedance feeding into the multiplexer by inserting a buffer amplifier in the line that would have a very high input impedance and a very low output impedance. The high input impedance of the amplifier would not "load down" the output from the sampling scope, and thus eliminate a possible source of distortion of the waveform. The very low output impedance of the amplifier would decrease the time necessary to charge up the capacitance of the cables and the assorted stray capacitances in the circuit. The second way is the method that was chosen.

Experimental Procedure

Before starting the data-taking program, the following procedure is used.

1. Turn on all the equipment (except the pulser) and allow it at least 30 minutes to "warm up," i.e., to come to thermal equilibrium.
2. Check the calibration of the system with a 2 ns standard (HP 226A Time Mark Generator), and adjust the horizontal sweeps of the oscilloscopes if necessary.
3. Turn on the pulser and obtain a pair of signals from the probe.
4. Adjust the delay in the B channel of the sampling unit plug-in so that the two signals occur simultaneously.
5. Using the DC offset and the Time Position adjustment knobs on the sampling scope, adjust the position of the waveform in the "data window" on the display of the monitor oscilloscope and remove the DC level.
6. Final adjustments of the position of the probe and the cables from it are made at this time. The probe is placed at a position near the model that corresponds to a position of a probe on the air-

craft. On the cylinders, various positions for the probes are used.

7. Using the counter (HP 5314A Universal Counter), measure the time necessary for the oscilloscope to complete ten sweeps and divide this number by ten. This number is the average time required for the oscilloscope to complete a sweep.

After these preliminaries are completed, type in the command R DATA. The machine will query back for the necessary information before running. The name of the output file, the settings on the sampling oscilloscope, and the current sweep rate of the system will be information required for the program to proceed. The program will take eleven consecutive sweeps, deleting the first sweep and keeping the last ten, and average them to obtain a single waveform. During the computer sampling, the counter should be left on in order to measure the time necessary for the eleven sweeps to be completed. If, due to a malfunction, the actual rate varies from the rate that was inserted in the program, the data should be purged from the records. There is always some small variation, typically 0.10 to 0.25 percent, which is acceptable.

Sensors

Two different sensors were used to make all the measurements of the electromagnetic field on both the model and the two cylinders. They were a D-dot and a B-dot probe. The B-dot probe is a model MGL-6A(R), manufactured by EG&G, having a bandwidth of at least 1.8 GHz [Ref. 8]. The D-dot probe is a model ACD-4A(R), also manufactured by EG&G, having a bandwidth of at least 1.1 GHz [Ref. 9]. A photograph of the sensors is given in Figure 2.

Cylinders and Model

Two different sizes of cylinders were used in the experiment. The first cylinder, hereafter referred to as the small cylinder, was 3 ft long and had a diameter of 2 in. The second cylinder, referred to hereafter as the large cylinder, was also 3 ft long, but had a diameter of 6 in. The ratio of diameter-to-length of the small cylinder was nearly the same as that used in theoretical work by Tesche [Ref. 5] and

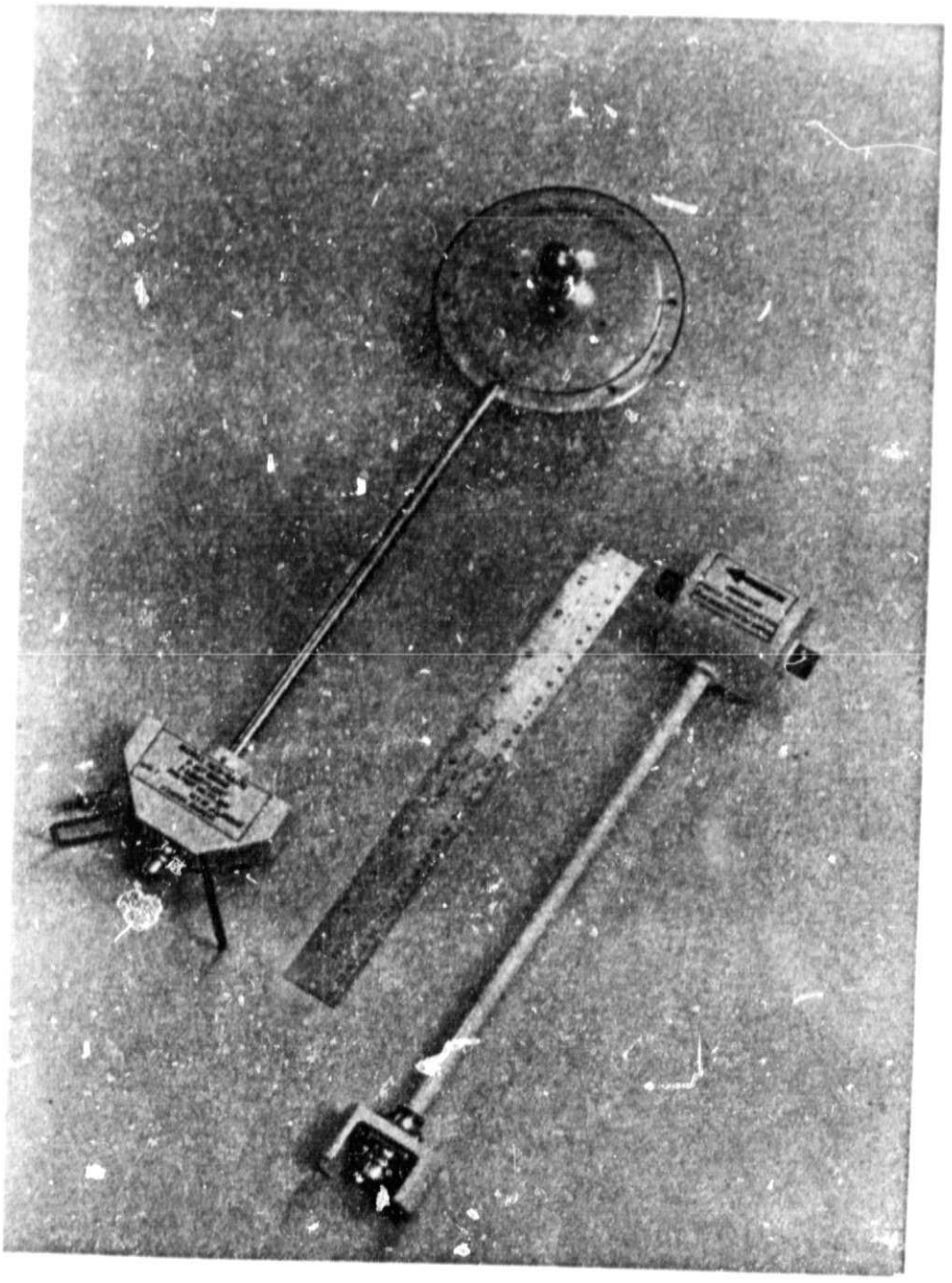

Figure 2. Photograph of the sensors.

by Yang [Ref. 6]. Some direct comparisons with their calculated poles are in Chapter III.

The aircraft model is an approximate model of an F-106B delta-wing aircraft. The model was constructed in the following manner. The fuselage was made of an aluminum cylinder, 2 ft long with a 4-in diameter, and an aluminum cone, 1 ft long with a base diameter of 4 in, tapering down to a diameter of 2 in. The tail and both wings were constructed of 1/16-in-thick brass and made to scale with the rest of the model. They were mechanically attached to the fuselage with screws, and to assure a good electrical connection, copper tape was also used. The overall scale of the model was 18.8:1. A comparison between the model and the actual aircraft is shown in Figure 3, and Figure 4 shows the model in the experimental setup.

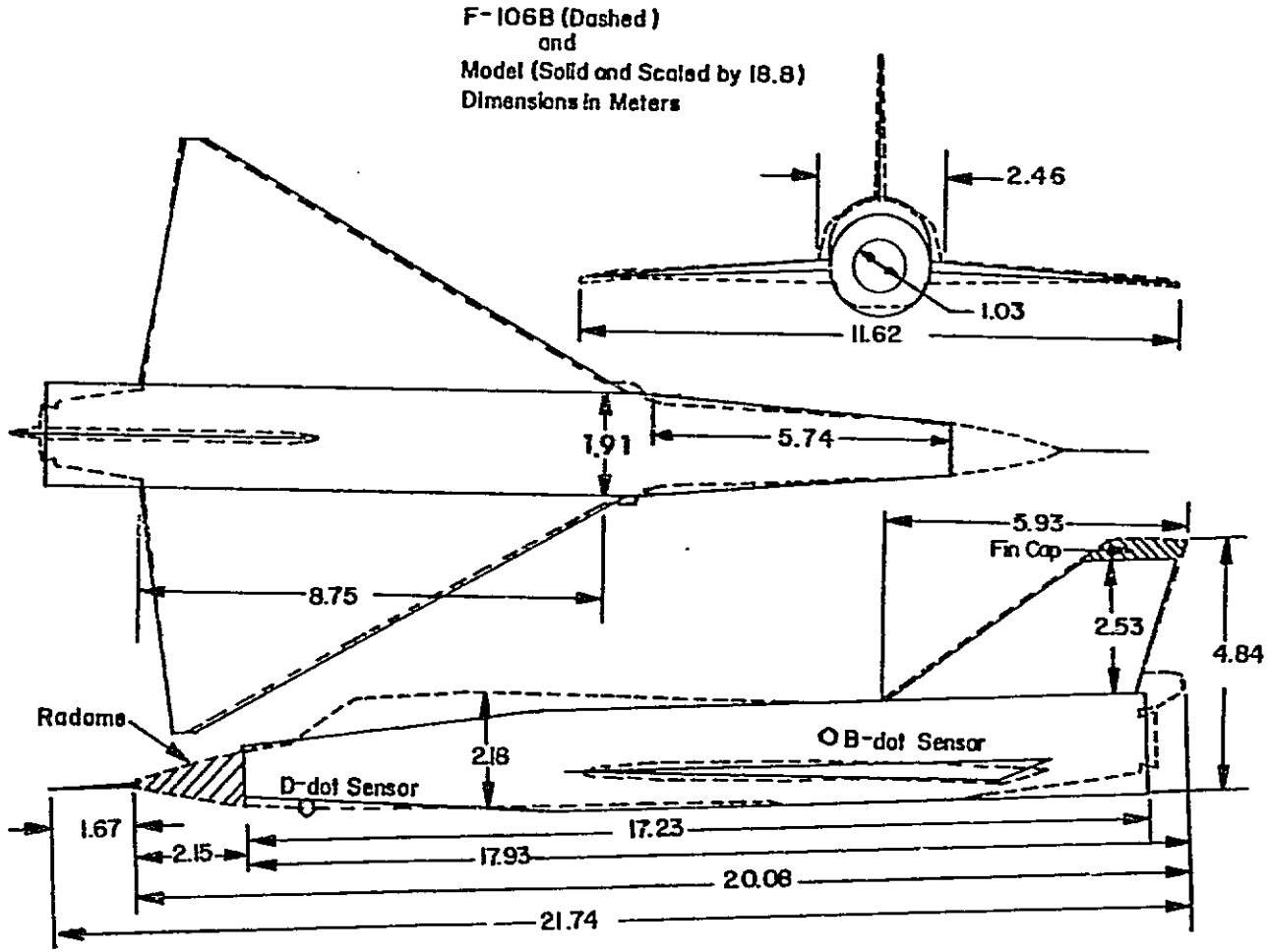

Figure 3. Scaled drawing of the model and the F-106B aircraft.

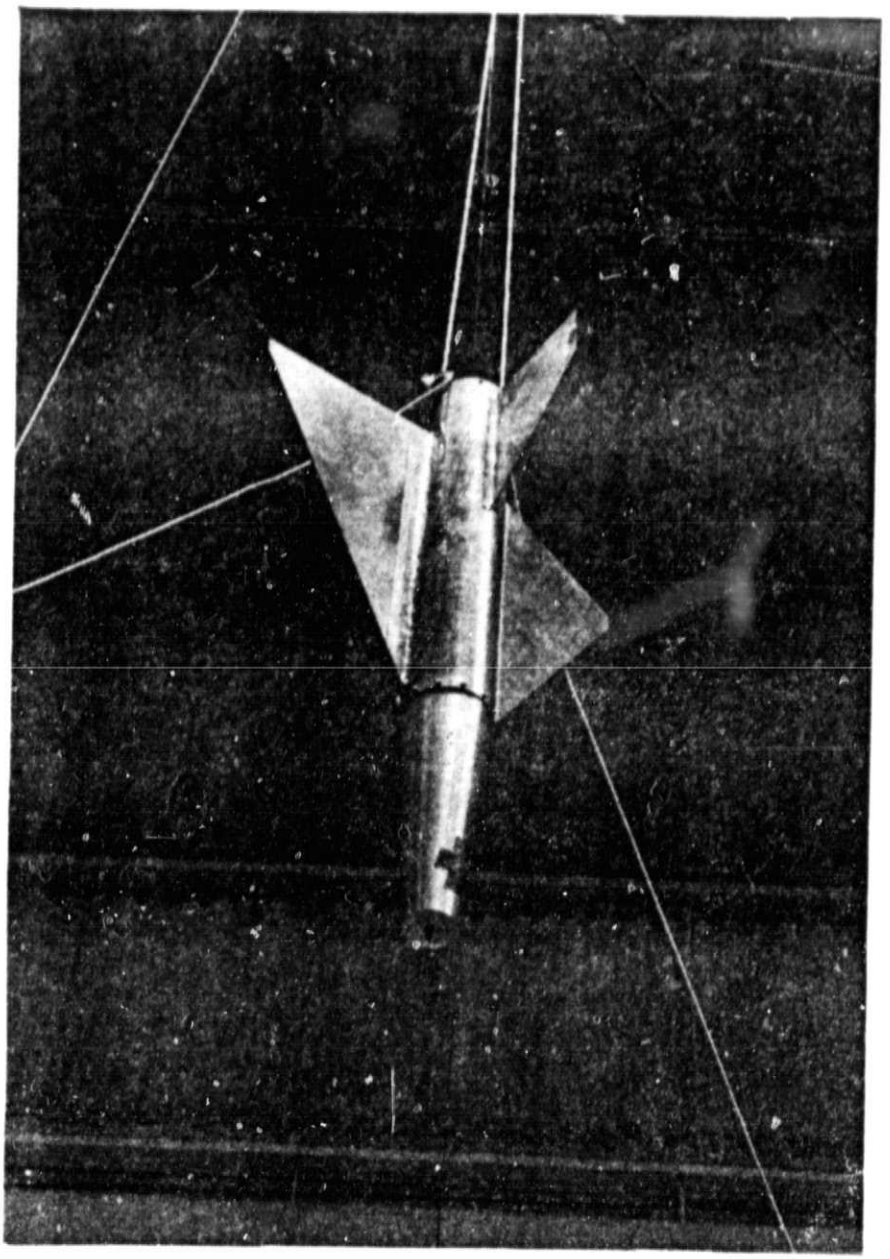

Figure 4. Photograph of the model.

III. RESULTS FROM THE CYLINDERS

Measurements of the natural frequencies of the cylinders were done first for comparison to previous cylinder work. By comparing the present results with those of Turner [Ref. 1], the degree to which the resistive wire affected the experiment was found, since Turner used the same cylinders but used the outer shield of 0.141-in semirigid coaxial cable for the wires. Comparisons with the theoretical calculations by Tesche [Ref. 5] and Yang [Ref. 6] were also interesting. The work by Tesche involved the natural frequencies of isolated cylinders, while the work by Yang dealt with the effect that a resistive wire attachment would have on the natural frequencies of a cylinder.

Both the magnetic field (B-dot) and the electric field (D-dot) were measured at the center, lengthwise, of the cylinders. As shown in Figure 5, the B-dot probe would "see" only the fundamental frequency and its odd harmonics, while the D-dot probe would measure only the even harmonics. By making the measurements in this manner, the two probes would complement each other. The D-dot probe was also moved to a second location on both of the cylinders in order to measure the odd harmonics for comparison with the B-dot results. The amount of agreement of the odd harmonics was taken as a measure of the accuracy of the technique. This second location was one-quarter of the length of the cylinder from the end.

A typical measured B-dot and D-dot response for the small cylinder is shown in Figure 6, and for the large cylinder in Figure 7. The input pulse that was used is given in Figure 8. Prony analysis was carried out as described in Reference 1. The only special processing that the waveforms received before being analyzed by the Prony program was a simple low-pass filtering that was done for two reasons. The first reason was to remove the chance of aliasing occurring in the Prony program. The second was to remove as much of the "white noise," generated by the sampling heads, as possible. The fundamental frequency of both cylinders was around 160 MHz, and the bandwidth of both probes was less than 2 GHz. The program that filtered the waveforms did so by

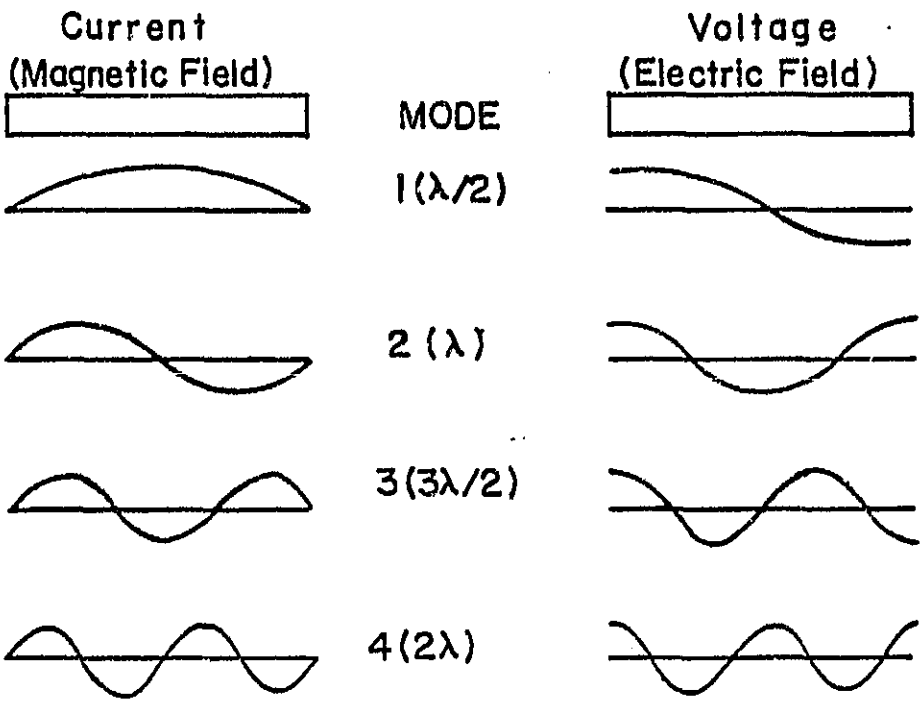

Figure 5. Modes of resonances for the cylinders.

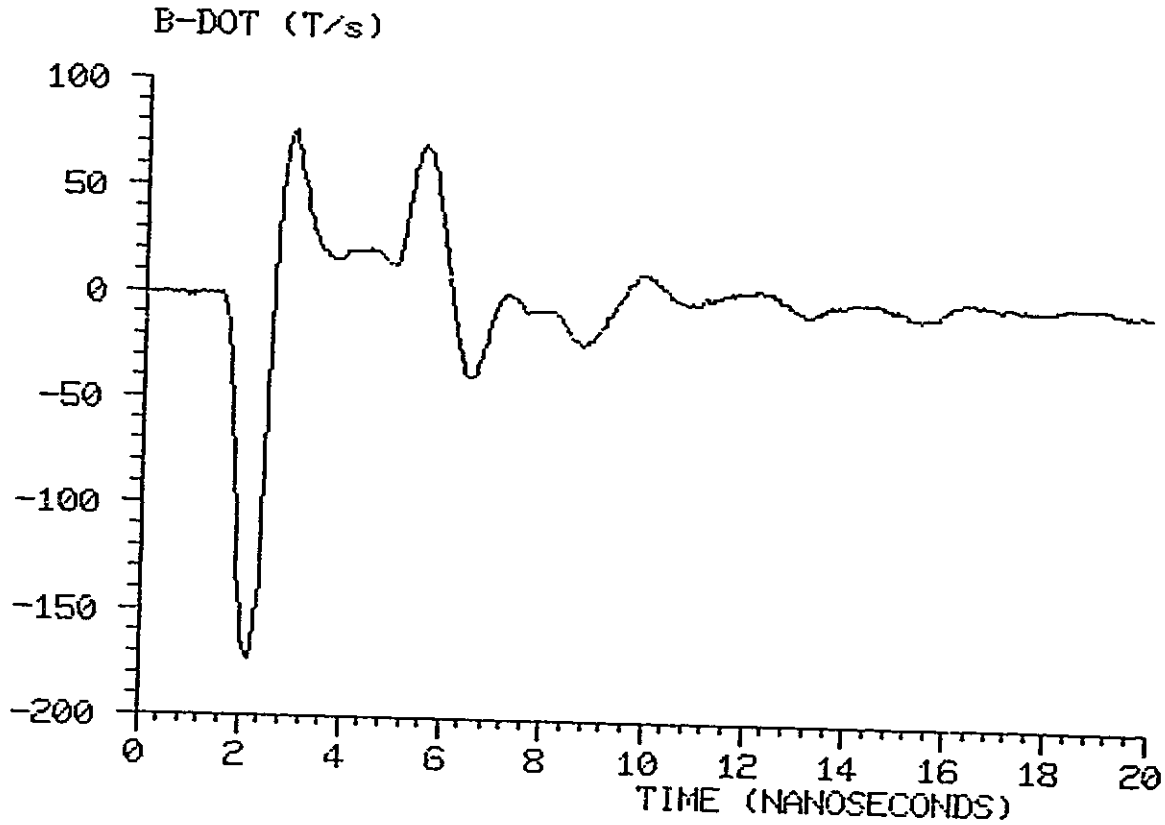

Figure 6. Waveforms recorded for the small cylinder.
(a) B-dot waveform.

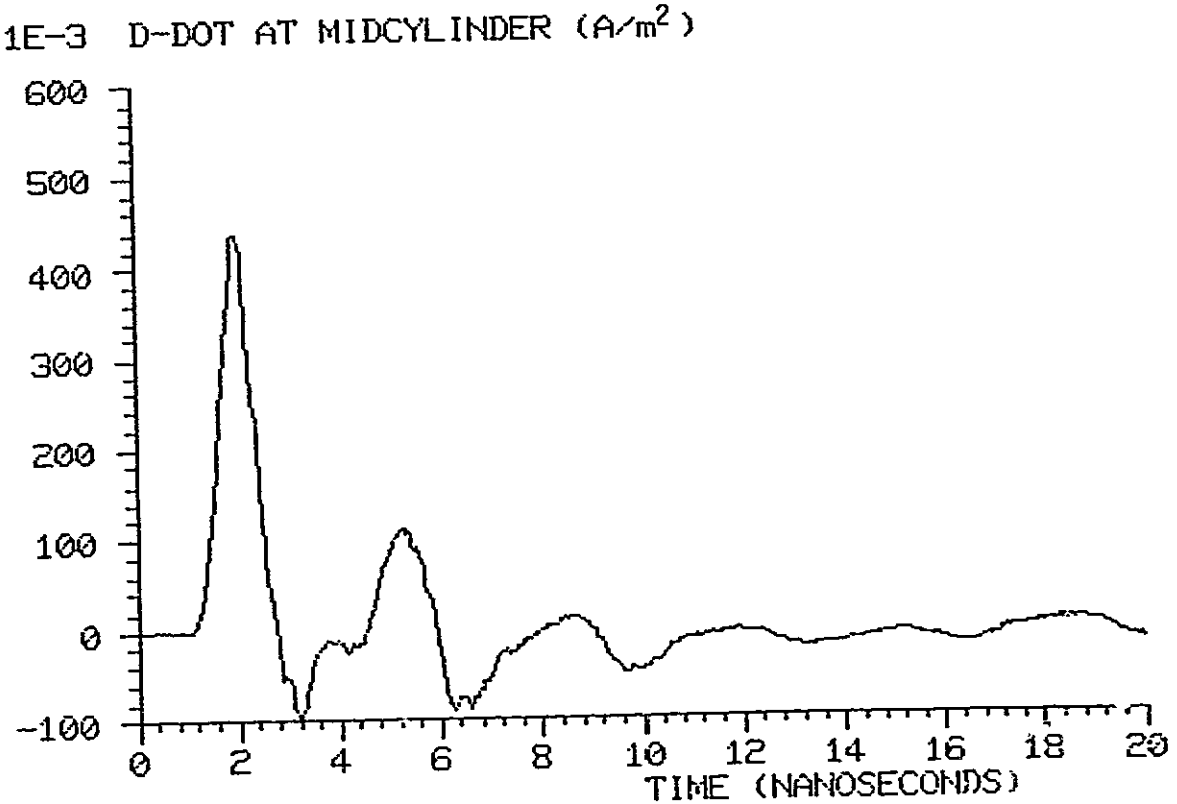

Figure 6. Waveforms recorded for the small cylinder.
(b) Midcylinder D-dot waveform.

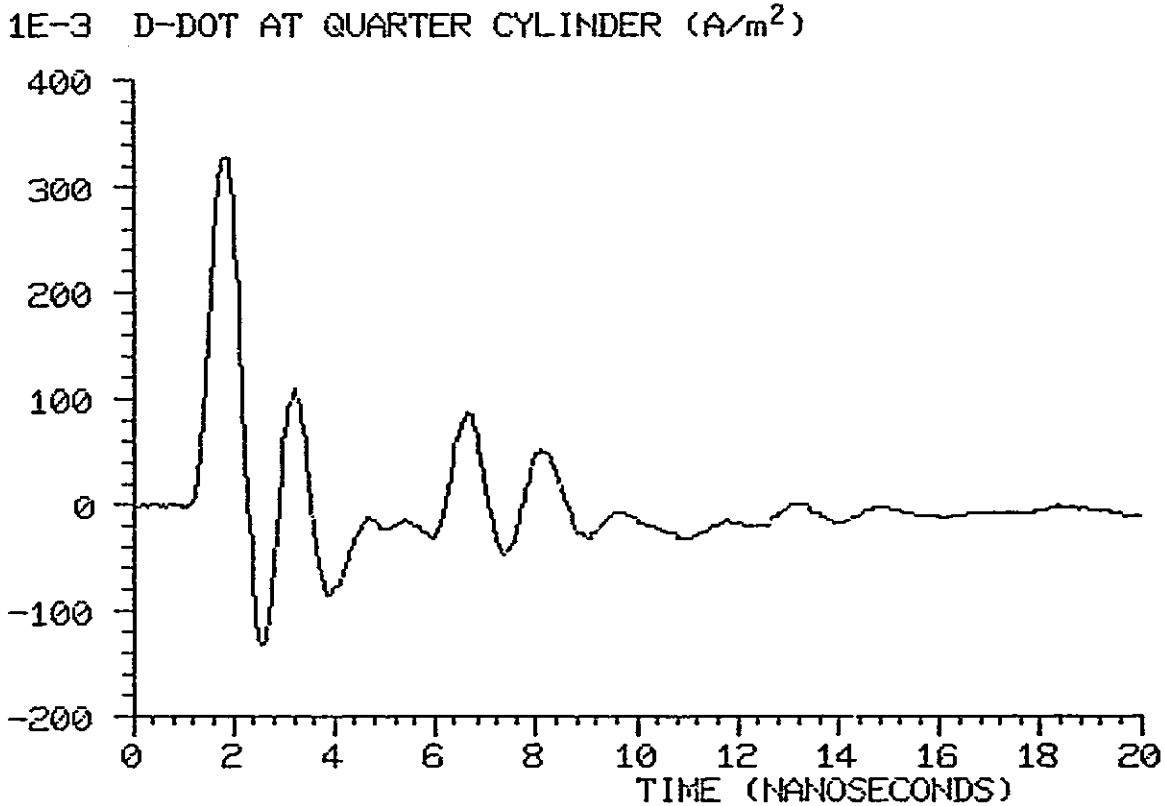

Figure 6. Waveforms recorded for the small cylinder.
(c) Quarter-cylinder D-dot waveform.

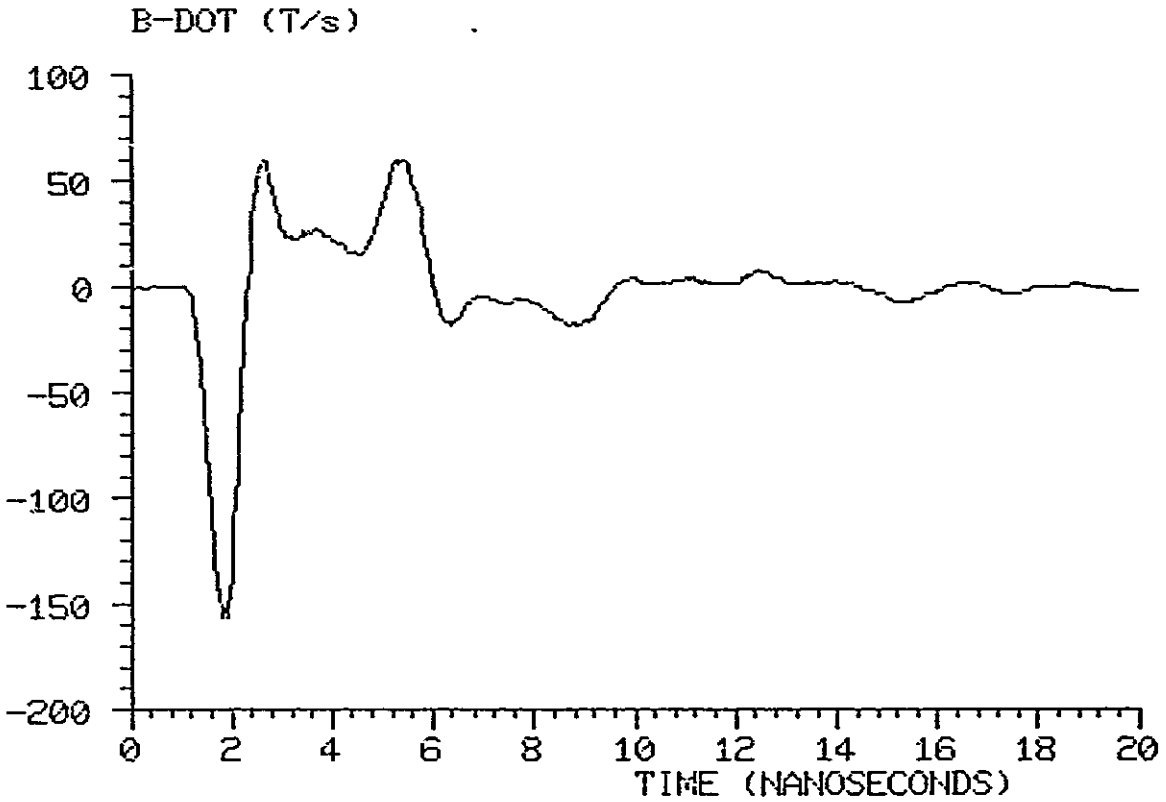

Figure 7. Waveforms recorded for the large cylinder.
(a) B-dot waveform.

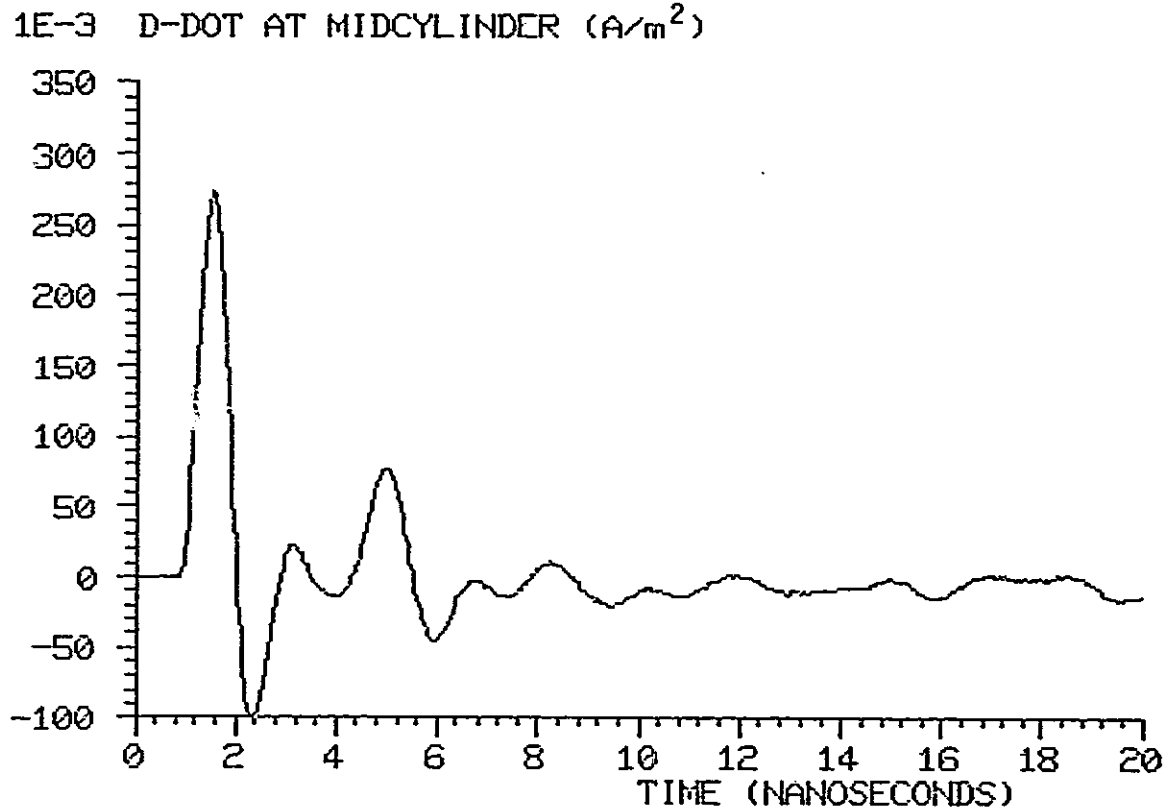

Figure 7. Waveforms recorded for the large cylinder.
(b) Midcylinder D-dot waveform.

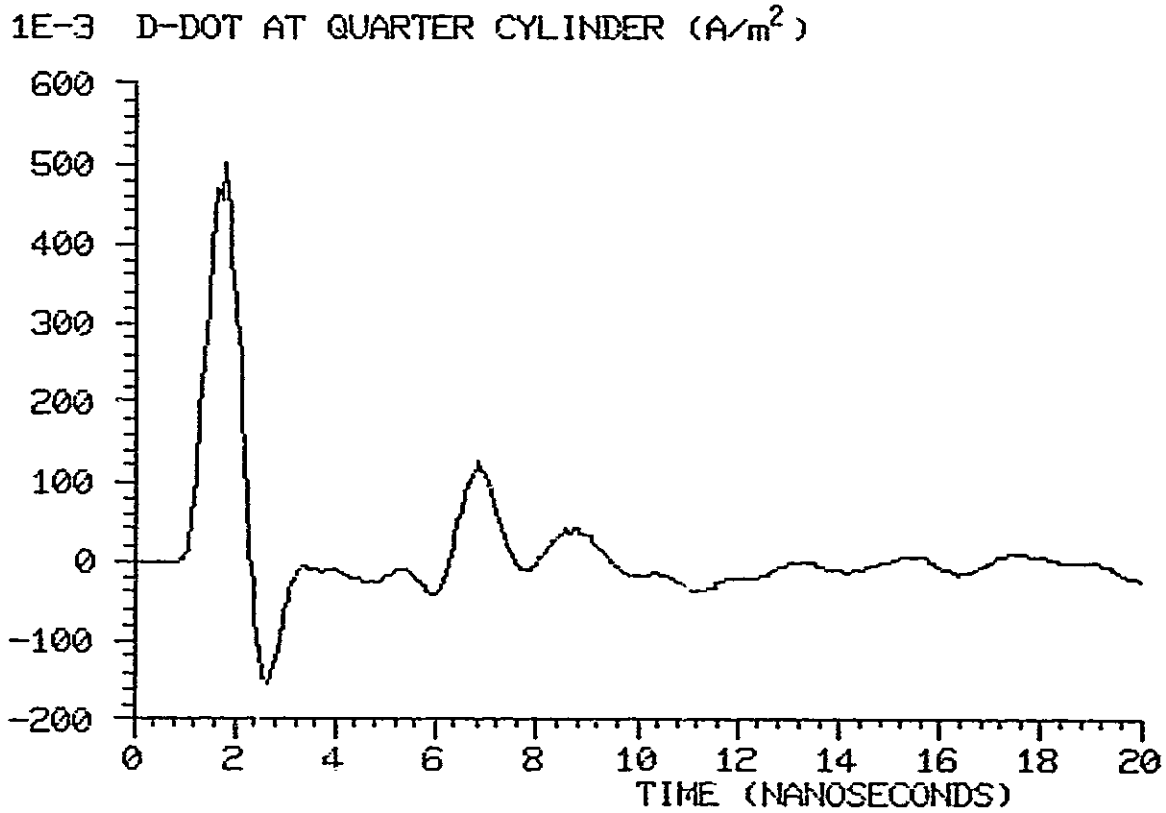

Figure 7. Waveforms recorded for the large cylinder.
(c) Quarter-cylinder D-dot waveform.

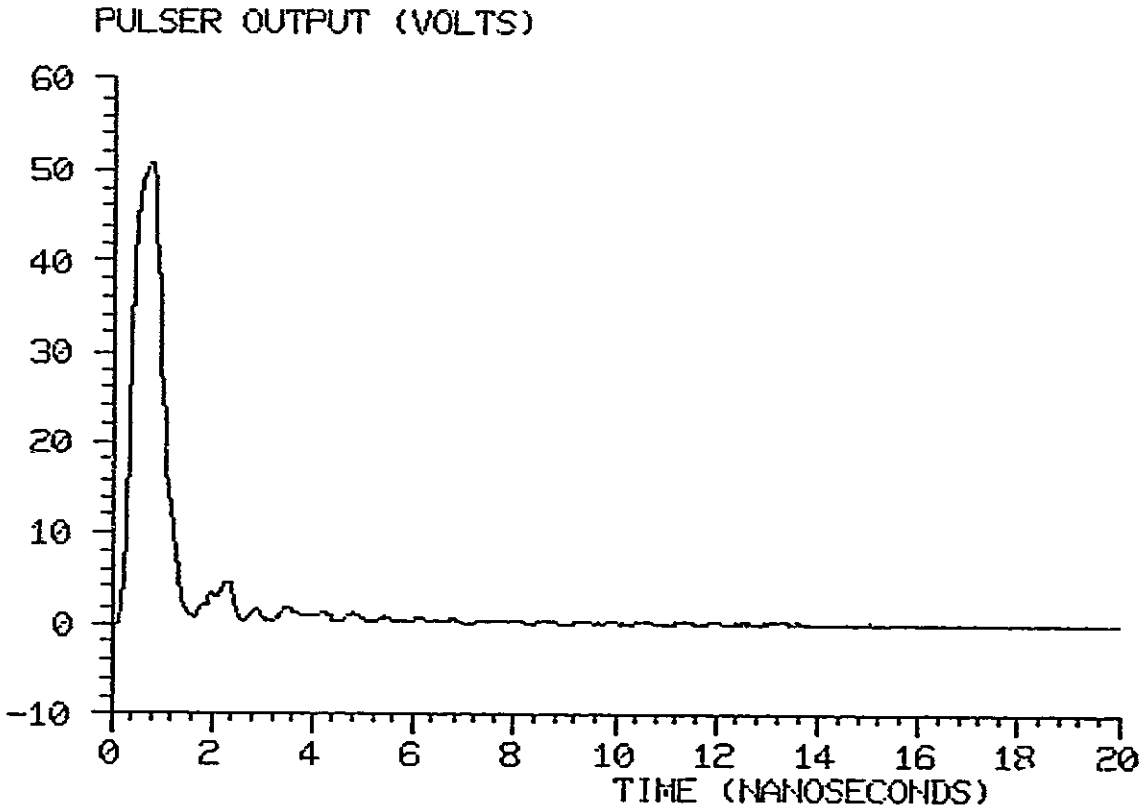

Figure 8. Input voltage waveform.

searching for a minimum in the frequency spectrum in the 2-GHz to 2.5-GHz band and making that the cutoff frequency.

The Prony poles have been normalized in the following way. The frequencies (in rad/s) and the damping rates (in Np/s) were multiplied by the length of the cylinder, L, and divided by the quantity of pi times the speed of light in vacuum. See, for example, the labels on the axes in Figure 9. The normalized frequency of the first resonance thus has a value near 1.0.

The results of the Prony analysis on both of the fields measured at the center of the small cylinder are given in Table 1. A Prony order of 18 with a sampling rate of every sixth point was used on the D-dot data. For the B-dot data, a Prony order of 18 was also used, but a sampling rate of every eighth point was used. In both cases the program was set to take ten time shifts. Thus the real poles could be discerned from the pseudopoles, created by the Prony program, on the basis of their stability. Only the poles from the reconstructions having an RMS error less than or equal to 6 percent were used to obtain the means and the standard deviations in the table.

TABLE 1. PRONY RESULTS FOR THE SMALL CYLINDER

Pole Number	Damping	Frequency	Probe
First	-0.231±0.004	0.920±0.000	B-dot
Second	-0.275±0.005	1.873±0.007	D-dot
Third	-0.304±0.005	2.741±0.004	B-dot
Fourth	-0.325±0.005	3.617±0.005	D-dot

The D-dot probe was also placed near the end of the small cylinder and the fields were measured. This was done, as mentioned above, so that there would be some overlap of the poles measured by both sensors. The results of this are given in Table 2. The B field data is the same as was given in the previous table; the new D-dot data has a Prony order of 24 and a sampling rate of every sixth point. The agreement

between the B-dot and D-dot poles is generally good with one exception, the frequency of the first pole.

TABLE .. A COMPARISON BETWEEN THE B-DOT AND THE D-DOT POLES OF THE SMALL CYLINDER

Pole Number	Damping	Frequency	Probe
First	-0.236±0.014	0.851±0.004	D-dot
	-0.231±0.004	0.920±0.000	B-dot
Third	-0.291±0.004	2.799±0.004	D-dot
	-0.304±0.005	2.741±0.004	B-dot

The different values that the two measurements gave for the frequency of the first pole was disturbing. There were two possible sources for this difference in the two waveforms. The first source was that the probes interacted with the fields of the cylinder and somehow either raised the frequency with the B-dot probe, or lowered the frequency with the D-dot probe. The second possible source was that of accumulated round-off error in the Prony program.

To examine this problem further, the waveforms were processed by a low-pass filtering program that was designed to just pass the first pole. The results are shown in Table 3. The agreement has now become excellent. From this, the conclusion is drawn that divergence of the first pole was due to round-off error.

TABLE 3. A DETAILED COMPARISON OF THE FIRST POLE

Probe	Frequency
B-dot	0.880±0.000
D-dot	0.880±0.000

The procedure used on the small cylinder was repeated on the large cylinder. First, the B-field and D-field were measured at the center of

the cylinder; then the D-dot probe was moved to the second location, near the end of the cylinder, and the D-field was recorded. In the analysis on the first set of data, the Prony order was set at 36 with a sampling rate of every sixth point for the B-dot waveform. For the D-dot waveform, the Prony order used was 24 and a sampling rate of every sixth point was used. In both cases the acceptable limit on the reconstruction error was set at 6 percent. The results are given in Table 4.

TABLE 4. PRONY RESULTS FOR THE LARGE CYLINDER

Pole Number	Damping	Frequency	Probe
First	-0.240±0.000	0.827±0.005	B-dot
Second	-0.290±0.000	1.769±0.003	D-dot
Third	-0.330±0.024	2.722±0.061	B-dot
Fourth	-0.347±0.005	3.480±0.007	D-dot

For the analysis of the D-field waveform measured near the end of the cylinder, a Prony order of 30 and a sampling rate of every sixth point were used. The results are given in Table 5. The agreement between the odd poles obtained from the two probes is very good.

TABLE 5. A COMPARISON BETWEEN THE B-DOT AND THE D-DOT POLES OF THE LARGE CYLINDER

Pole Number	Damping	Frequency	Probe
First	-0.240±0.000	0.827±0.005	B-dot
	-0.242±0.004	0.830±0.012	D-dot
Third	-0.330±0.024	2.722±0.061	B-dot
	-0.324±0.005	2.656±0.012	D-dot

A comparison between the poles generated by the two cylinders is provided in the graph of Figure 9. In this graph, the odd poles are the average of the poles from the B and D fields. The most noticeable

difference in the poles is the lower frequencies of the larger cylinder. This is due to the increased capacitance of the end plates of the cylinder. The lowering of the frequency of resonance is more pronounced in the higher modes. A second effect of increasing the diameter of the cylinder is a slightly stronger damping of the pole.

A comparison with the results of Turner [Ref. 1] for both cylinders is given in Table 6 and in Figures 10 and 11. In Figure 10 the small cylinder results are compared, and in Figure 11 the large cylinder results are compared. The wires used by Turner were the copper outer shield of 0.141-in semirigid coaxial cable; they have a much lower resistance than those used in the present study as well as a larger diameter.

TABLE 6. A COMPARISON WITH TURNER'S WORK

Turner		With Resistive Wire Attachment	
Small	Large	Small	Large
-0.394+j0.980	-0.273+j0.869	-0.234+j0.880	-0.241+j0.829
-0.407+j1.960	-0.310+j1.750	-0.275+j1.873	-0.290+j1.769
-0.395+j2.840	-0.359+j2.643	-0.298+j2.770	-0.327+j2.689
-0.403+j3.840	-0.370+j3.473	-0.325+j3.617	-0.347+j3.480

The table shows that the damping is much higher for the cylinders with a nonresistive attachment (Ref. 1). How the frequency is affected by the resistivity of the attachment is a bit unclear. A clearer picture of the effects of the wires can be obtained from the graphs. In Figure 10 the change in the damping rate for the small cylinder is very pronounced. There is also a change in the frequency between the two cases. In the work done with the copper wire attachment, the frequencies were higher, and even more so in the higher modes. For the large cylinder in Figure 11, the differences between the poles are much smaller. The poles obtained from the experiment in which the copper

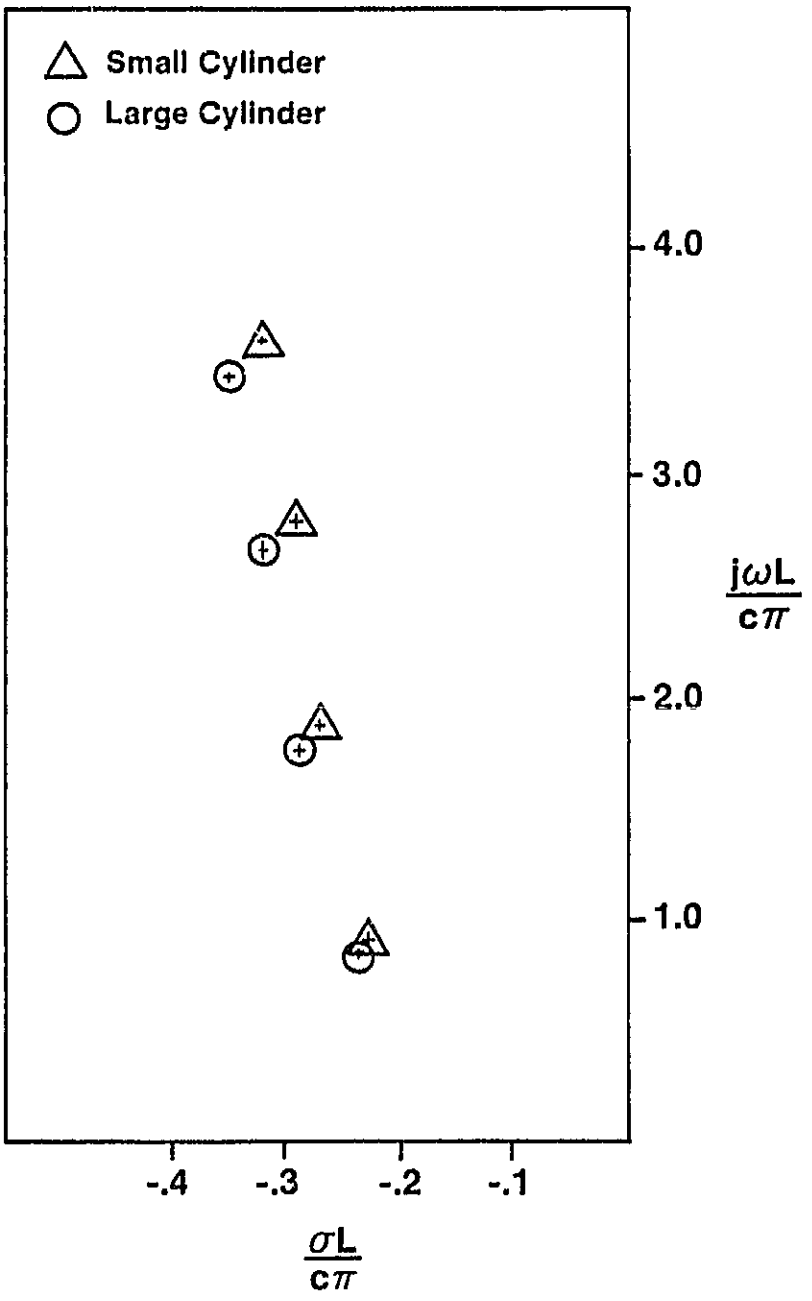

Figure 9. A comparison between results from the two cylinders with resistive wires.

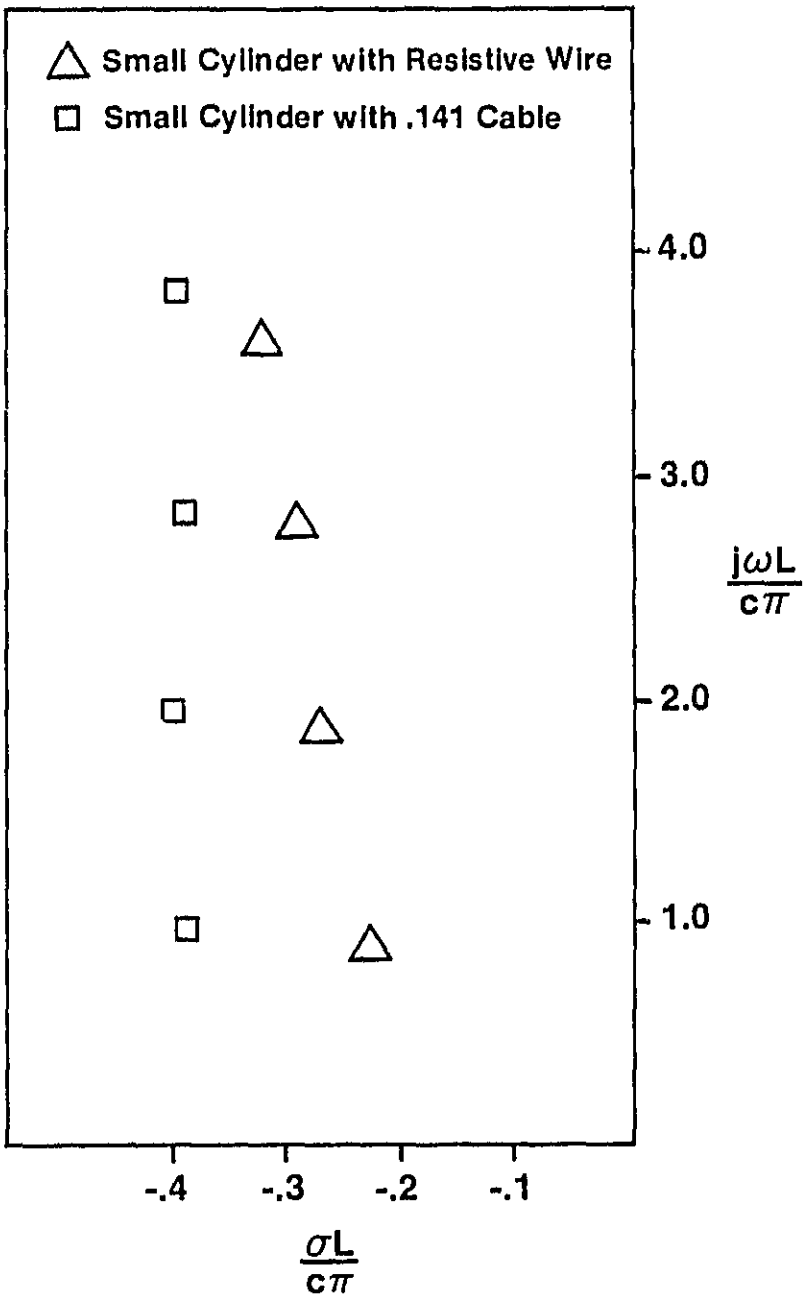

Figure 10. A comparison between the small cylinder results.

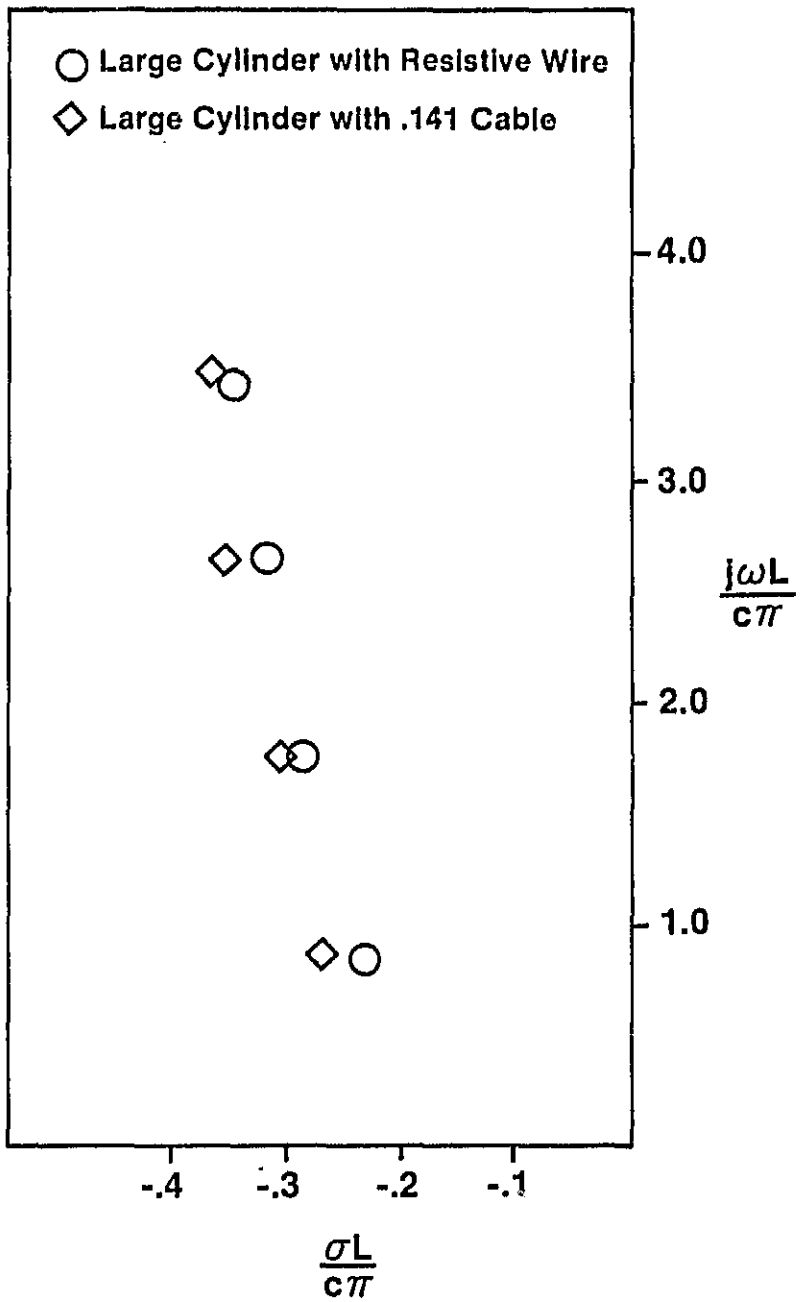

Figure 11. A comparison between the large cylinder results.

wires were used have a slightly, though consistently, higher damping rate. The effect that the larger, more conductive wires have on the frequency is negligible.

Theoretical work by Tesche [Ref. 5] covers the scattering of an electromagnetic field by an isolated cylinder having the same dimensions as the small cylinder used in this experiment. Yang [Ref. 6] has performed calculations for the scattering by a cylinder which has a resistive wire attached. The ratio of the dimensions of the cylinder (cylinder diameter/cylinder length) and the wire attachment (cylinder diameter/wire diameter) in Yang's work are close to those of the small cylinder used in this experiment. Yang calculated the resonances when the resistivity of the wire was 2.51 Ω/ft and when it was 2513 Ω/ft. Yang's model could calculate only the odd harmonics of the cylinder. Table 7 gives a comparison between our measured results for the poles and the results the two computer models predicted.

TABLE 7. A COMPARISON WITH SOME THEORETICAL WORK

Pole Number	Source	Damping	Normalized Freq.
First	Yang (2.51 Ω/ft)	-0.291	0.926
	Measured (8 Ω/ft)	-0.234	0.880
	Yang (2513 Ω/ft)	-0.152	0.870
	Tesche (Isolated case)	-0.104	0.860
Third	Yang (2.51 Ω/ft)	-0.361	2.963
	Measured (8 Ω/ft)	-0.298	2.770
	Yang (2513 Ω/ft)	-0.239	2.778
	Tesche (Isolated case)	-0.205	2.742

The table shows that the damping for the poles from the experiment lies between the damping calculated by Yang for the two different wires. These same results can be seen in the graph of the poles provided in Figure 12.

This section on the resonances of cylinders could not be concluded without a comparison of the results of the Prony analysis with the results obtained from doing a fast Fourier transform on the waveforms. Figures 13 and 14 give the magnitudes of the Fourier spectra of the B-dot and the D-dot waveforms, respectively. The resonances are revealed as prominent peaks in the spectra. The locations of the peaks should, and do, agree approximately with the frequencies of the poles in the tables. For example, consider the poles, $-0.234 \pm j0.880$ and $-0.298 \pm j2.770$, listed in Table 7. In Figure 13(a), the peaks corresponding to these poles lie at about 0.158 GHz and 0.459 GHz; when normalized, these values become 0.963 and 2.755, demonstrating the approximate agreement. One must keep in mind that the basic frequency resolution of the Fourier transform is $(20\ ns)^{-1}$, or 0.05 GHz, which is not terribly good.

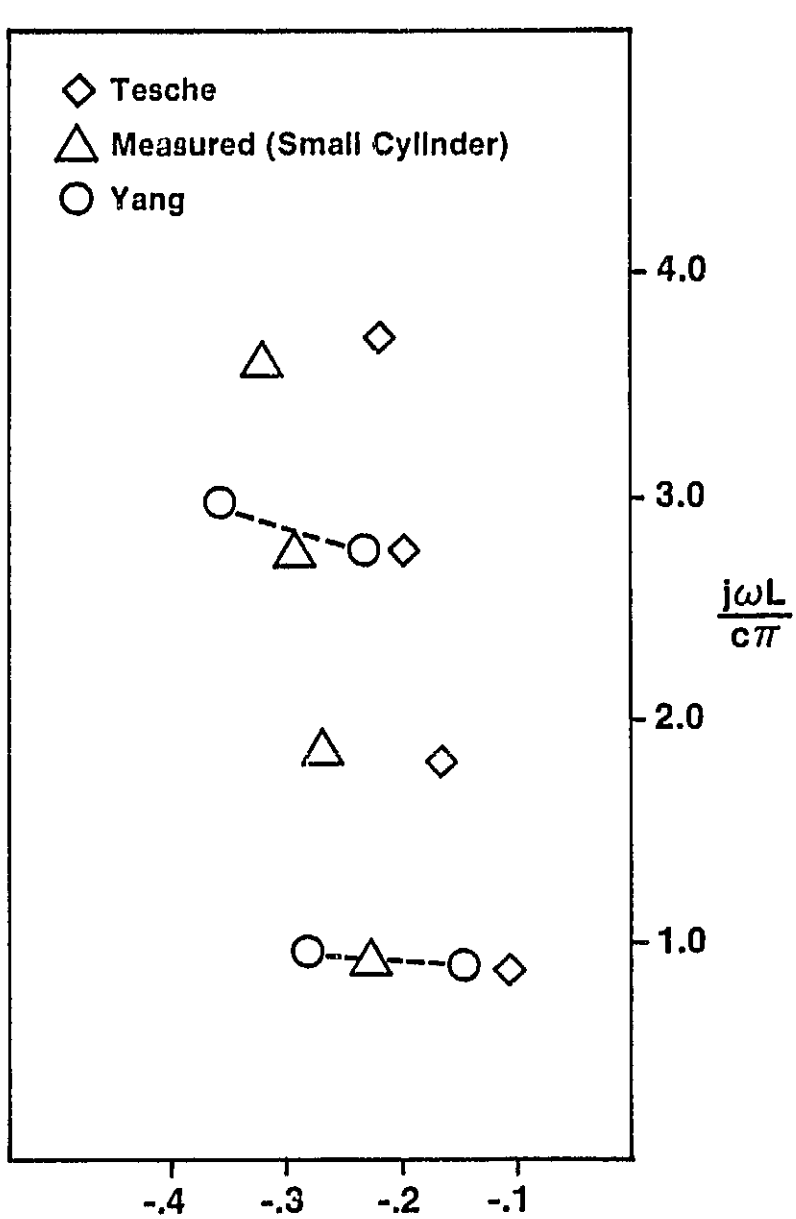

Figure 12. A comparison between the measured results and those calculated by different computer models.

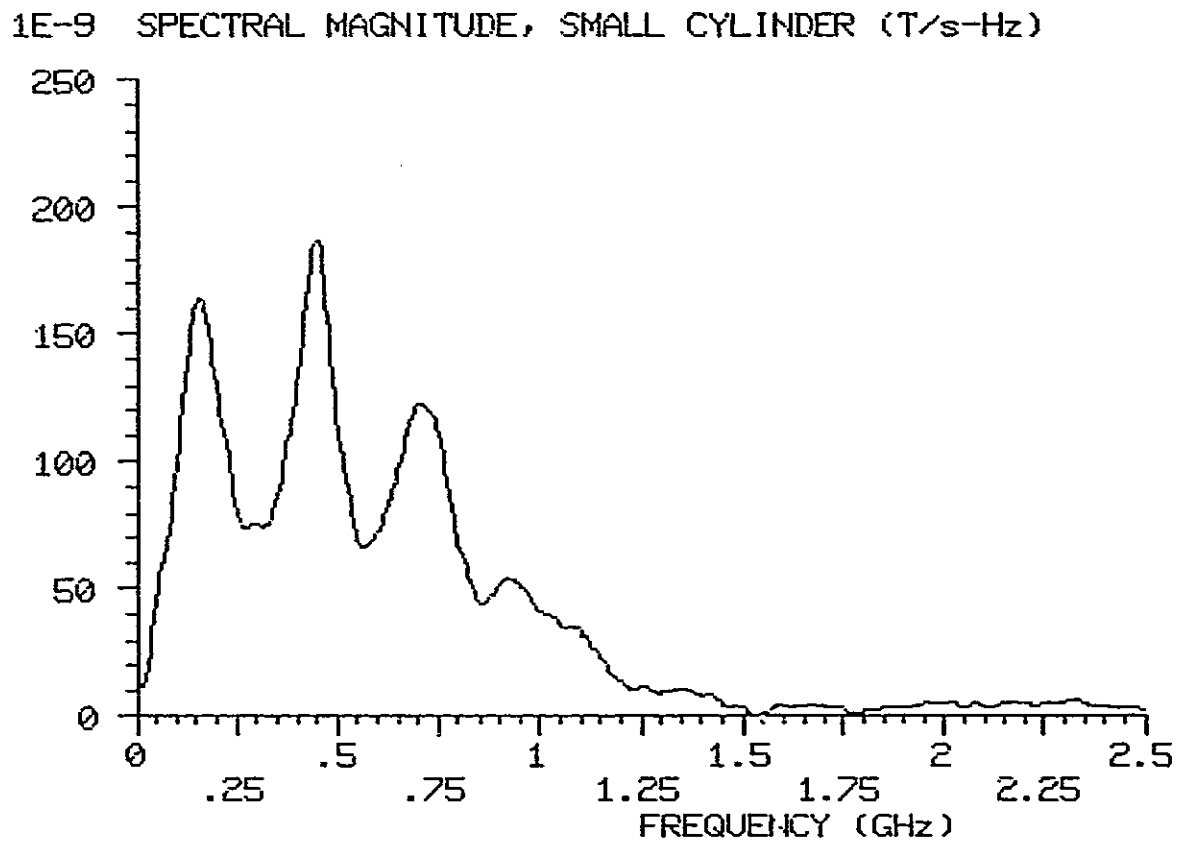

Figure 13. Fourier spectra of the B-dot waveforms from the cylinders. (a) Small cylinder.

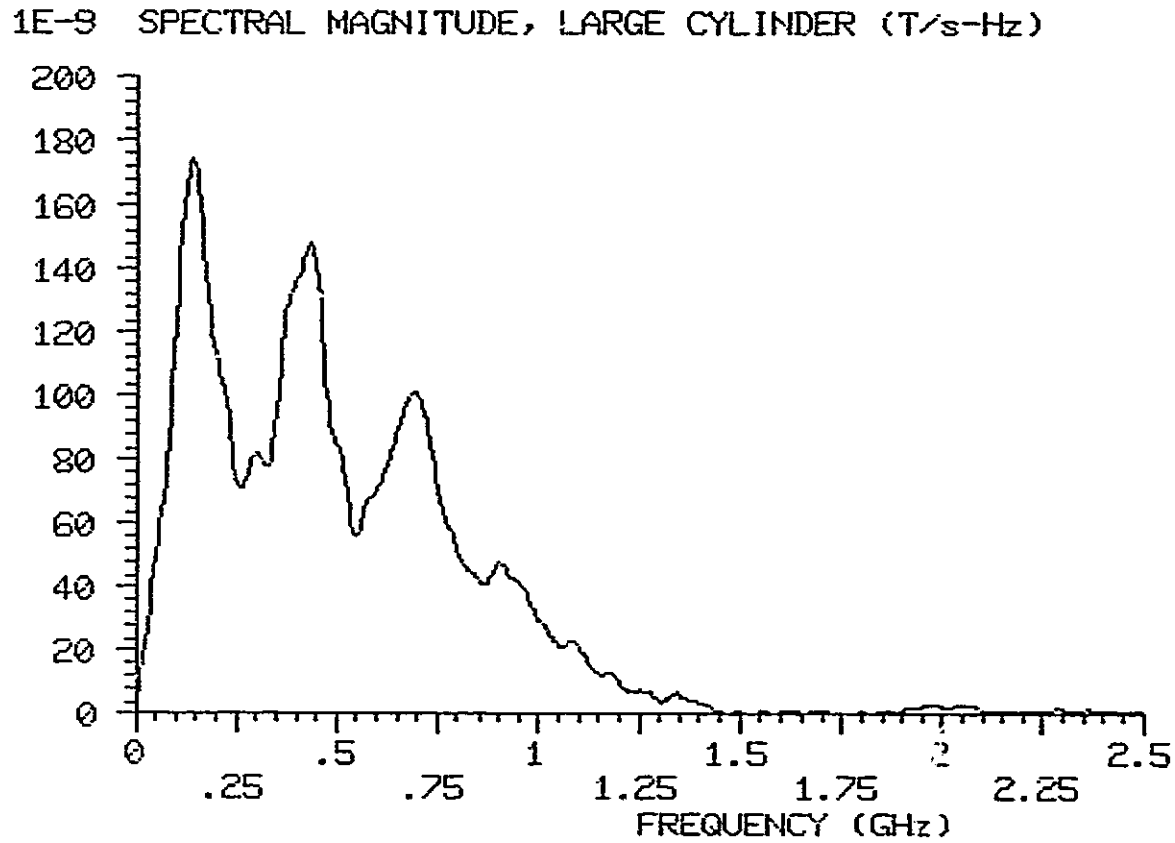

Figure 13. Fourier spectra of the B-dot waveforms from the cylinders. (b) Large cylinder.

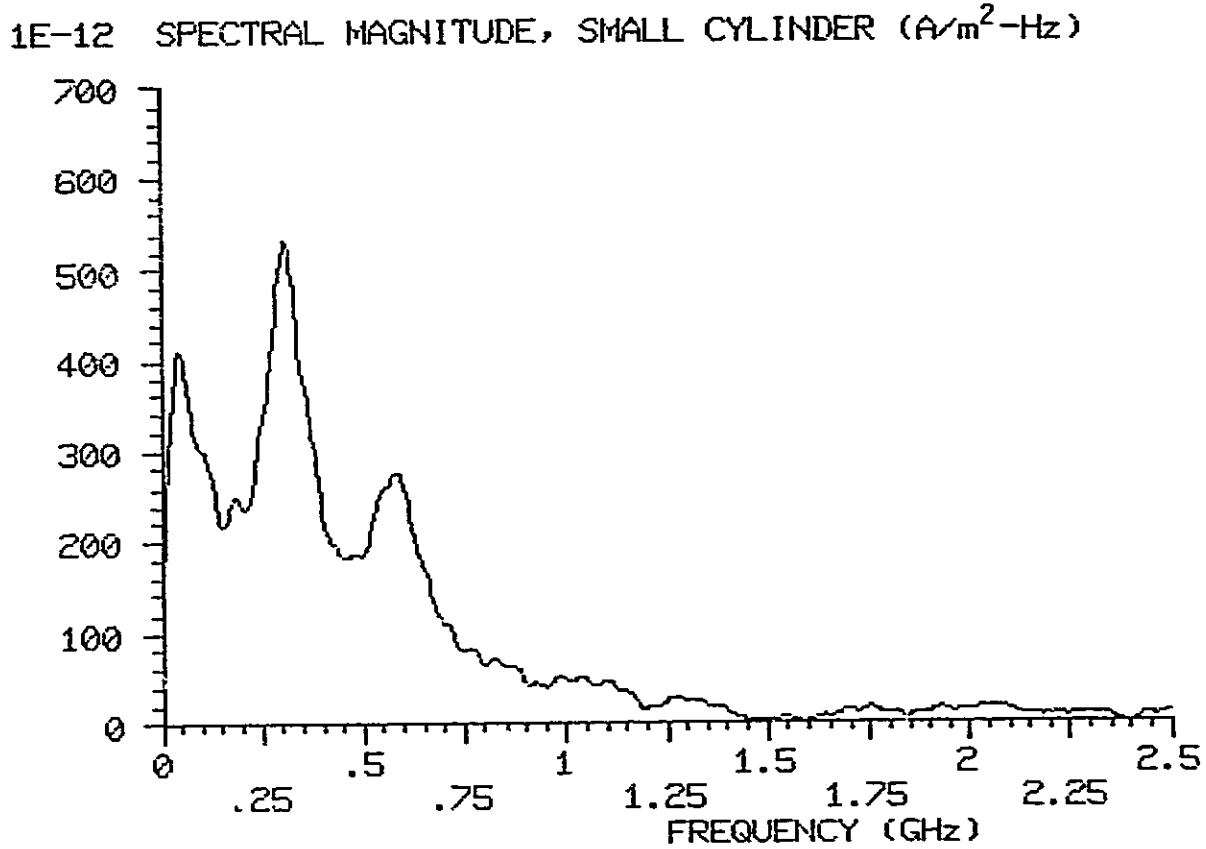

Figure 14. Fourier spectra of the D-dot waveforms from the cylinders. (a) Small cylinder.

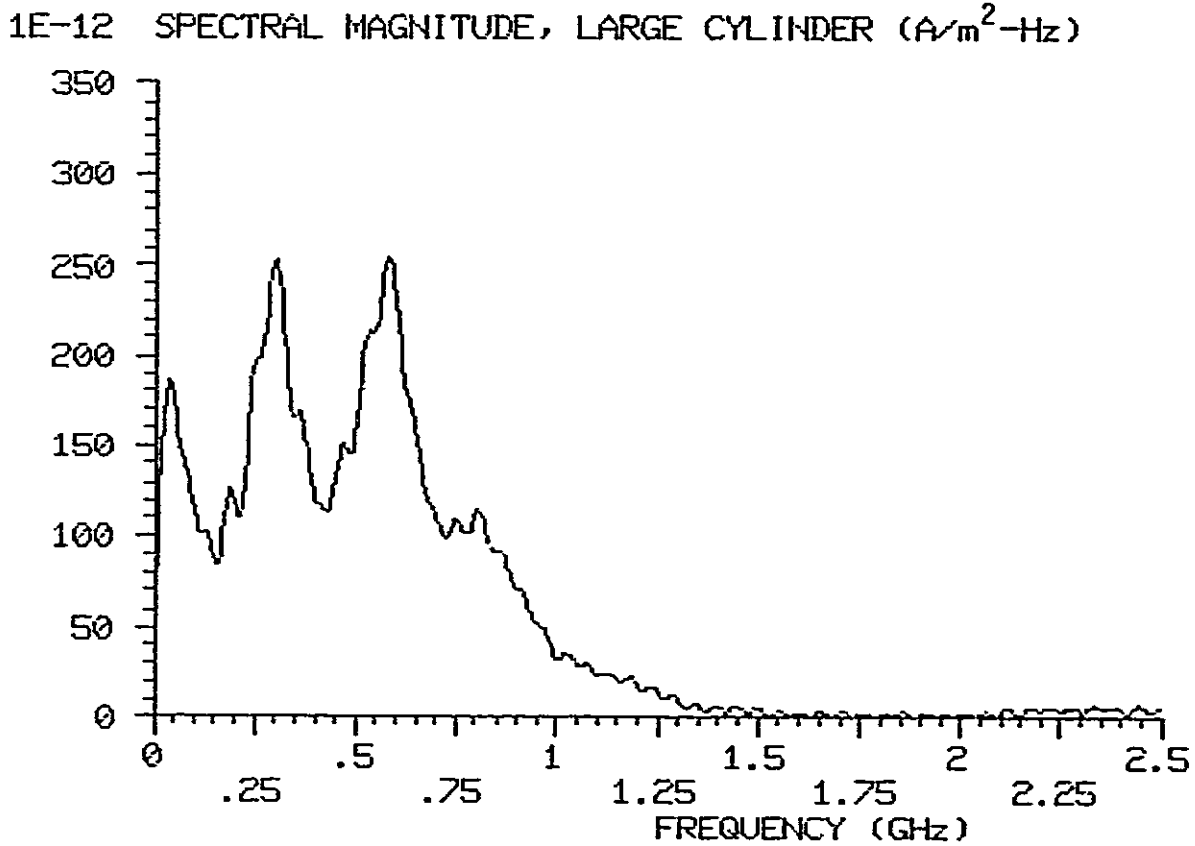

Figure 14. Fourier spectra of the D-dot waveforms from the cylinders. (b) Large cylinder.

IV. RESULTS FROM THE F-106B AIRCRAFT MODEL

Time domain reflectometry was used to test the experimental setup with the aircraft model in place. The output of the TDR was expected to show the large-scale structure of the experiment: the junction of the 50-Ω cable to the ground plane/resistive wire, the junction of the model to the resistive wire at both ends of the model, and the junction of the resistive wire to the ordinary wire that runs back to the ground. Because of the dissipative nature of the resistive wire, the fine detail of the model was expected to be lost in TDR. As shown in Figure 15, these expectations proved true.

The probes were positioned near the model so that they would correspond to the positions of the equivalent probe on the aircraft. The D-dot probe was placed at the underside of the model and just above the tip of the nose. The B-dot probe was located on the topside of the model just above the seam where the wing joins the fuselage. The magnetic field was nonuniform in this region, and the dimensions of the probe were of the same order as the gradient of the field. Because of this, the output of the probe corresponds to the average field inside the volume of the probe. Typical waveforms recorded from the D-dot and B-dot probes are given in Figures 16 and 17, respectively.

The damping rate of each pole was normalized as in the previous chapter, but the frequency of each pole was scaled downward so that a direct comparison could be made with the results of the actual aircraft. The frequency in this case was divided by 6.28318 to convert it from radians/second to Hertz, and then it was divided by 18.8 to scale it to the full-size aircraft.

The only special signal processing applied to the D-dot waveform was its passing through a simple low-pass filtering program. The reasons for filtering the waveform are the same as in the previous section. A Prony order of 24 and a sampling rate of every eighth point was used. For obtaining the mean and standard deviation, only reconstructions with an error rate less than 4 percent were used. The results are given in Table 8.

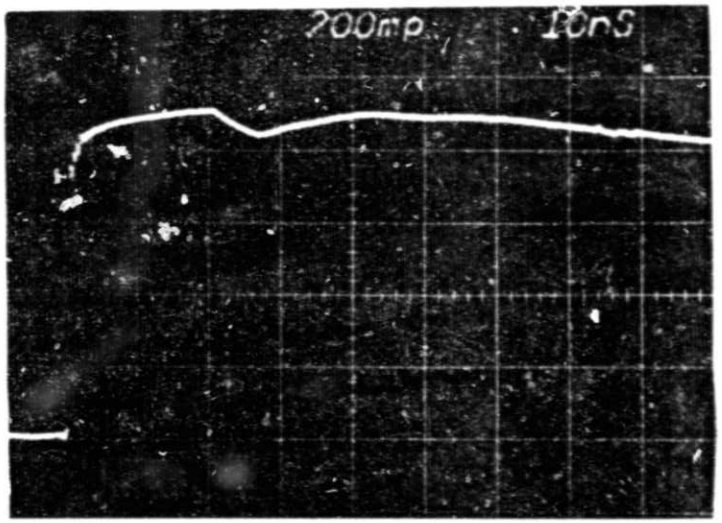

(a) TDR of the complete experiment.

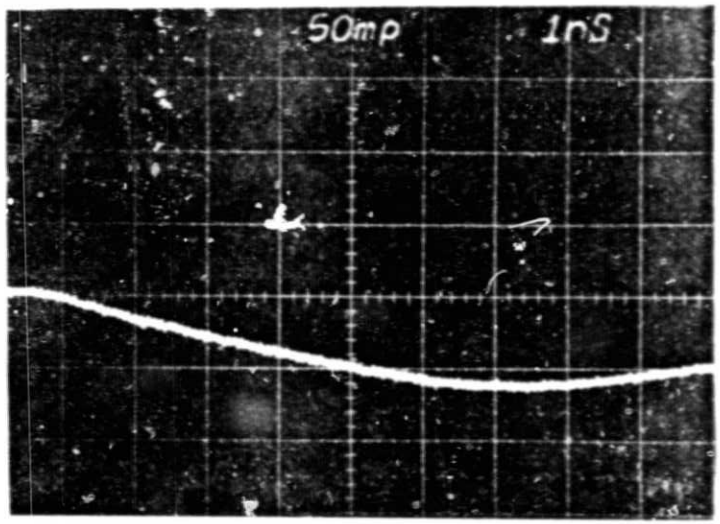

(b) Detail TDR of the model.

1. Junction between the 50 Ω cable and the ground plane.
2. Junction between the lower resistive wire and the nose of the experimental model.
3. Junction between the tail of the experimental model and the upper resistive wire.

Figure 15. TDR of the model in the experiment.

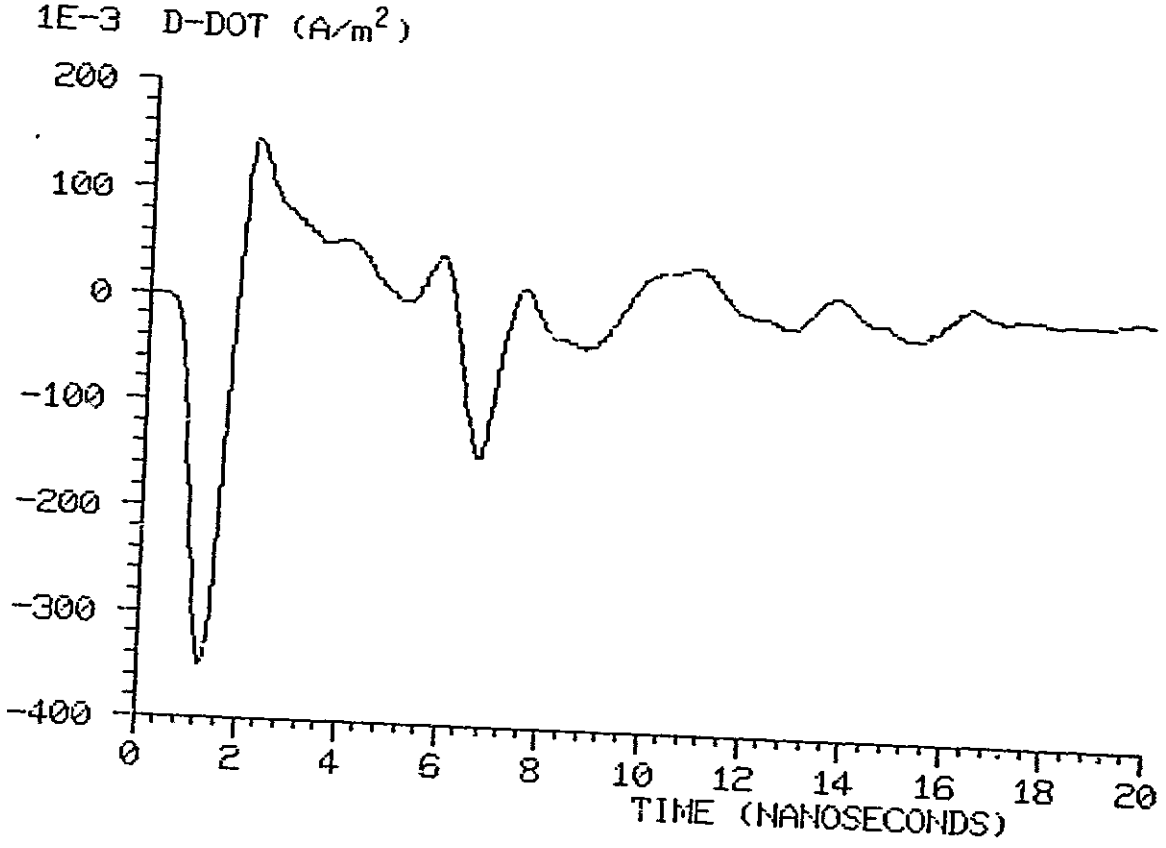

Figure 16. Typical D-dot waveform from the model.

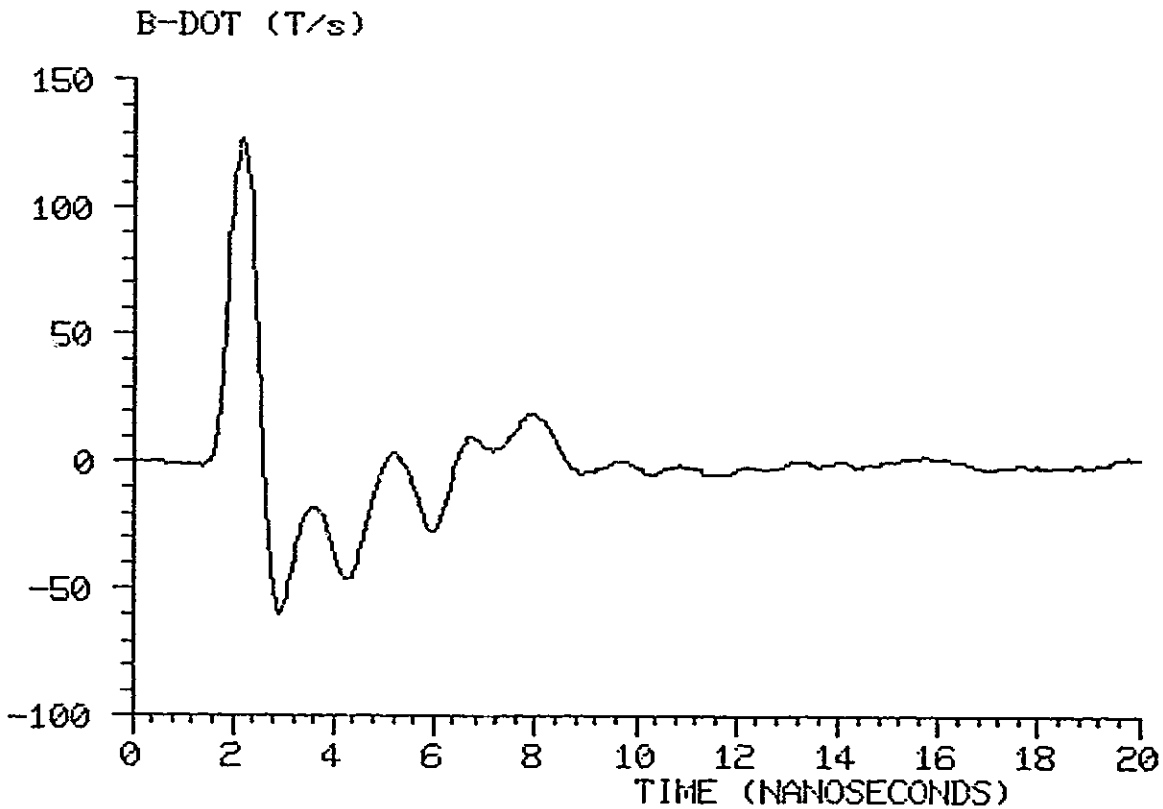

Figure 17. Typical B-dot waveform from the model.

TABLE 8. PRONY RESULTS FOR THE MODEL D-DOT WAVEFORM

Pole Number	Damping	Scaled Frequency (MHz)
First	-0.265±0.020	7.308±0.082
Second	-0.249±0.005	14.752±0.239
Third	-0.179±0.005	18.420±0.045
Fourth	-0.206±0.005	25.604±0.039
Fifth	-0.349±0.007	30.720±0.032
Sixth	-0.196±0.012	36.295±0.106
Seventh	-0.156±0.023	40.703±0.735

In Figure 18, the graph gives the frequency spectrum obtained from analyzing the waveform with a digital fast Fourier routine. Note the correlation between the results of the two methods (Prony and Fourier) of obtaining the frequencies of the poles in the D-dot waveform. In the Fourier results, five of the poles present in the Prony results are distinct, while two are hidden.

The analysis of the waveform recorded by the B-dot probe is a more complicated matter. When the usual filtering and analysis routine was run on this waveform, the first, second, sixth, and seventh poles were quickly resolved. The third and fourth poles were much slower in resolving into separate poles. Starting at a Prony order of 24 and various sampling rates, the first group of poles, first, second, sixth, seventh, were resolved and stable; but the third and fourth poles appeared to be a single pole. The frequency of this combined pole was the average of the third and fourth poles, and the damping rate was roughly the sum of the damping rates of the two poles. As the Prony order approached 36, the maximum that the computer could run, the two poles could just be seen to resolve into two separate poles. Due to the limit on the Prony order, the best way then available to resolve these two poles was to separate them from the rest. The waveform was processed by a program that simulated a bandpass filter, and the filtered waveform was used in the Prony analysis to find the third and fourth

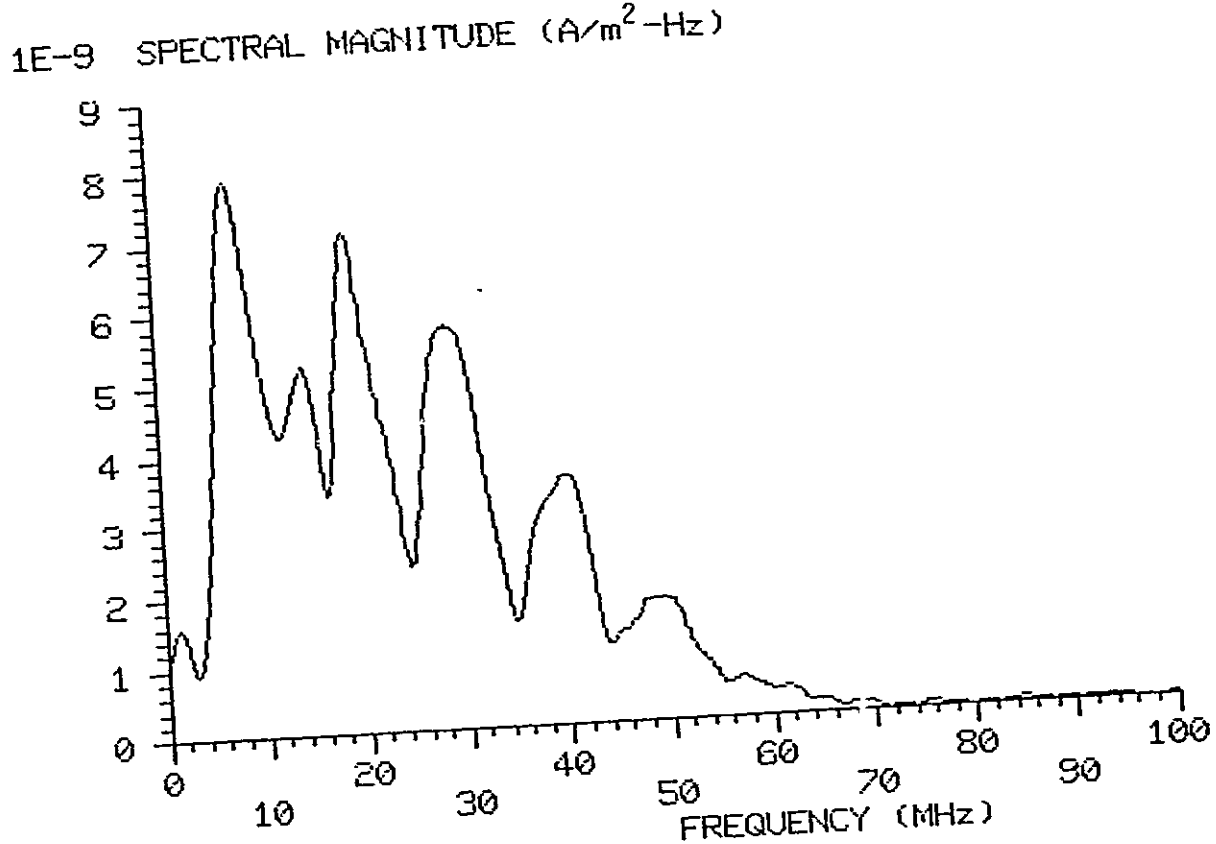

Figure 18. Fourier spectrum of the D-dot waveform from the model.

poles. The program examined the spectrum of the unfiltered waveform and passed only the frequencies between the first minimum after the second pole and the first minimum before the sixth pole.

For the waveform that contained all of the poles, the first, second, sixth, and seventh poles were obtained along with a combined third-fourth pole. The combined pole was not used. A Prony order of 24 with a sampling rate of every sixth point was used on this waveform. The percent of error (6 percent) on the reconstruction was a bit higher on the Prony of this waveform, but the poles were stable. The third and fourth poles were obtained from the bandpassed waveform. The Prony order used with this waveform was 20, with a sampling rate of every eighth point. The upper error limit for the reconstructions used to obtain the mean and standard deviation on these two poles was 1.5 percent. The Prony results are given in Table 9 along with a graph from the fast Fourier program in Figure 19.

TABLE 9. PRONY RESULTS FOR THE MODEL B-DOT WAVEFORM

Pole Number	Damping	Scaled Frequency (MHz)
First	-0.270±0.000	7.710±0.009
Second	-0.225±0.007	14.844±0.029
Third	-0.185±0.007	18.690±0.069
Fourth	-0.258±0.010	22.697±0.070
Fifth	Not Present in the B-dot Waveform	
Sixth	-0.200±0.009	36.139±0.030
Seventh	-0.051±0.003	39.326±0.055

A comparison between the two sets of poles will give a measure of the exactness of the results. There are only two poles, the fourth and seventh, that have a significant difference. The problem with the seventh is the difference in the damping rates. The seventh pole in the B-dot waveform was very weak. The Prony program has difficulty in

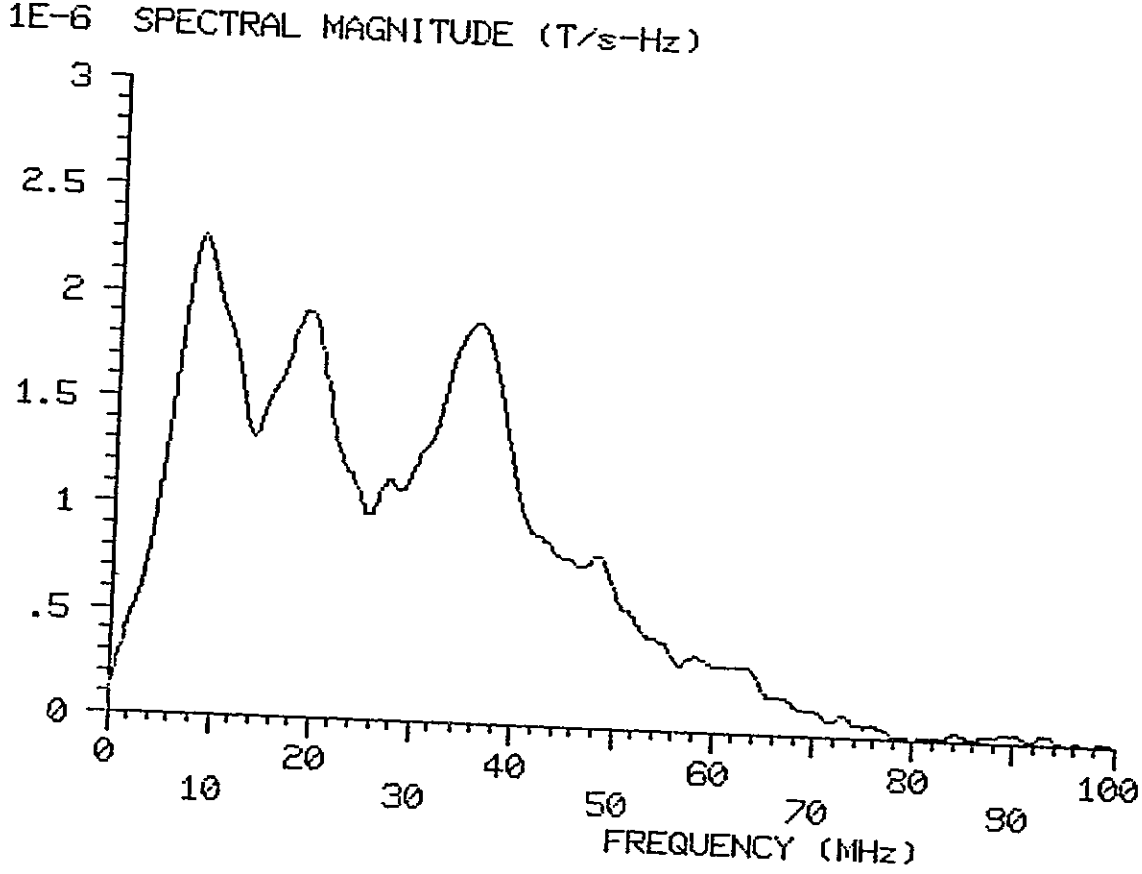

Figure 19. Fourier spectrum of the B-dot waveform from the model.

calculating the damping of a weak pole in the presence of a strong pole. Only the frequencies of the seventh pole will be compared, and the damping rate of the pole from the D-dot waveform will be taken as the true one. The fourth pole in both the B-dot and the D-dot waveforms is strong. The difference in the poles in this case is a difference of both the frequencies and damping rate.

The two sets of poles, B-dot and D-dot, are displayed in the graph in Figure 20. In Table 10, the differences in the two sets of poles are given. In this table, the percent difference between corresponding pole parts is calculated as the difference between them divided by their average. The differences are seen to be generally quite small.

TABLE 10. A COMPARISON BETWEEN THE B-DOT AND THE D-DOT PRONY RESULTS

Pole Number	Difference in the Damping	Difference in the Frequency
First	0.00	0.400 MHz
	0.0 %	5.326 %
Second	0.02	0.090 MHz
	8.333 %	0.608 %
Third	0.01	0.270 MHz
	5.405 %	1.455 %
Fourth	0.05	2.900 MHz
	21.277 %	12.008 %
Sixth	0.00	0.160 MHz
	0.0 %	0.442 %
Seventh	Not Compared	1.370 MHz
		3.424 %

In comparing the Prony results from 1982 in-flight waveforms [Ref. 7] against those of the model, a correlation between the pole sets can be seen. The comparison is given in both Table 11 and Figure 21. The model poles were averaged from the B-dot and D-dot poles. For the first two poles, the damping rate and the frequency of the poles from

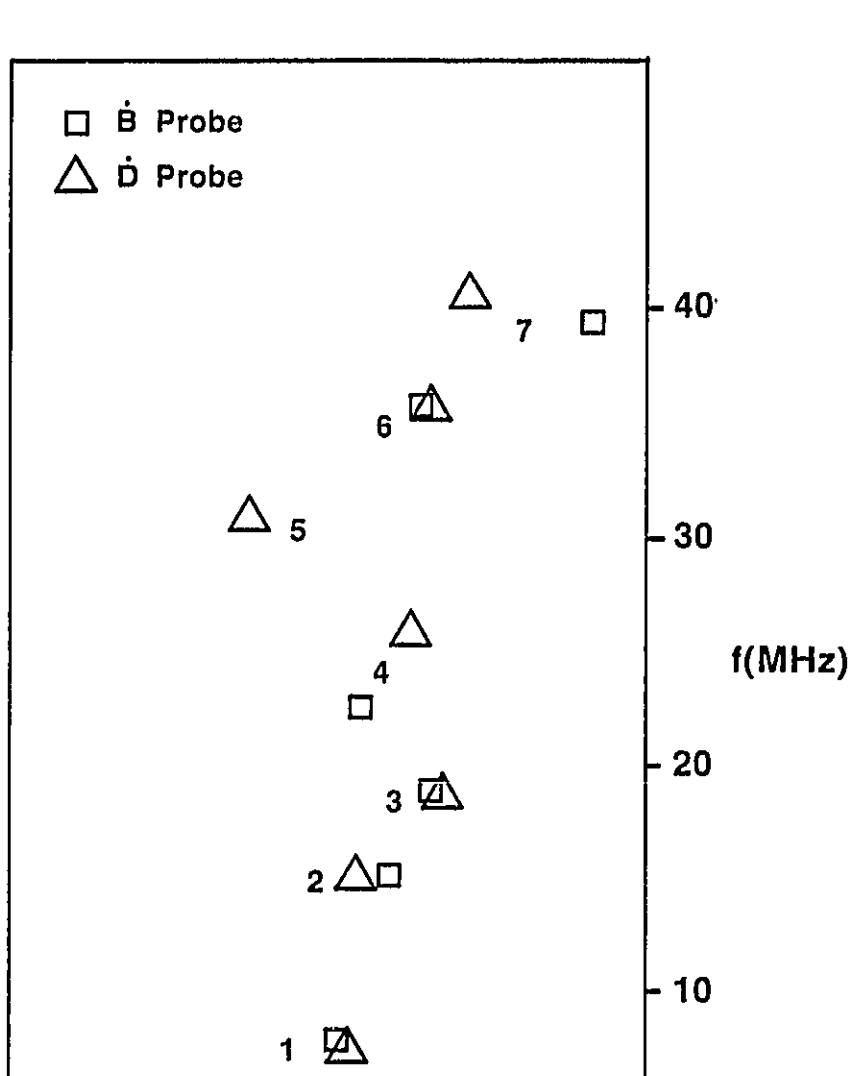

Figure 20. A comparison between the B-dot and the D-dot results.

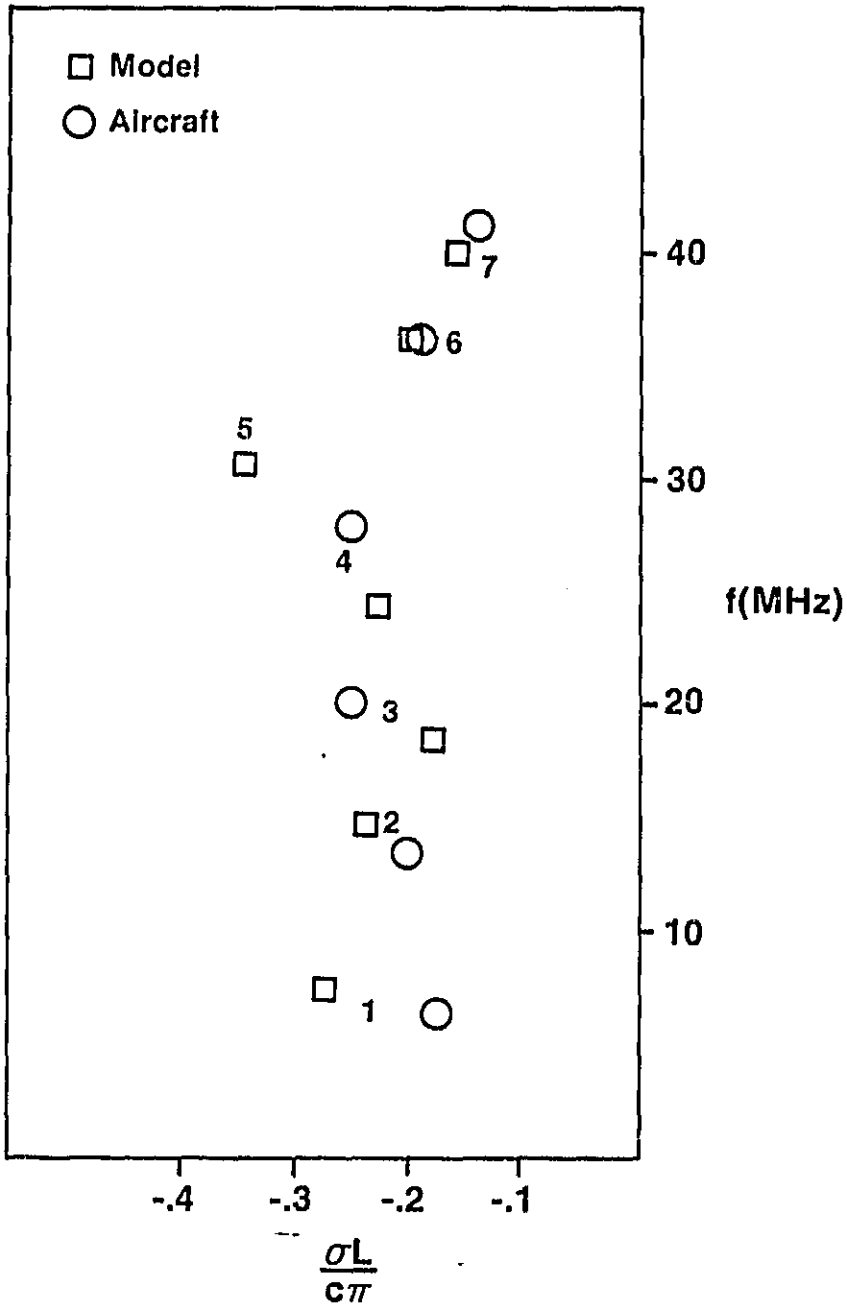

Figure 21. A comparison between the model and the aircraft results.

the model were higher than those from the airplane. This trend was reversed on the next pole. With the third pole, the damping rate and the frequency of the pole of the aircraft was higher than that of the model. The fourth pole of the aircraft had a considerably higher frequency than did the model, and a moderately higher damping rate. The aircraft did not have a pole that corresponded to the fifth pole generated by the model. For the last two poles, the sixth and seventh, the poles from the model had a slightly higher damping rate and a lower frequency than those from the aircraft. Overall, the approximate F-106B model with the simple wire model used for the lightning channel worked reasonably well.

TABLE 11. A COMPARISON BETWEEN THE MODEL AND THE AIRCRAFT RESULTS

	F-106B Model		Actual Aircraft	
Pole Number	Damping	Scaled Freq. (MHz)	Damping	Scaled Freq. (MHz)
First	-0.27	7.51	-0.18	6.50
Second	-0.24	14.80	-0.20	13.55
Third	-0.18	18.56	-0.25	20.55
Fourth	-0.23	24.15	-0.25	28.05
Fifth	-0.35	30.72		
Sixth	-0.20	36.22	-0.19	36.40
Seventh	-0.16	40.01	-0.14	41.40

The experimental model used in previous work [Ref. 1] differed from the model used in this work in several aspects. The first difference was in the model of the lightning channel. Previously the model was connected to the experiment with the copper outer shield of a 0.141 semirigid cable. A wire with a much smaller diameter and a higher resistivity was used in the present work to lower the damping of the poles on the model, thus bringing the damping into agreement with the aircraft results. The second difference was at the nose of the air-

craft. The earlier model had a blunt nose, while the model used in this experiment utilized a tapered one to achieve a more exact representation of the aircraft. One result expected from tapering the nose was a slight rise in the damping rates, because the taper of the nose would act as a transformer, matching the impedance of the rest of the model to the wire. By matching the impedances, the reflection coefficient is lowered, resulting in increased damping of the waveform.

As can be seen in Table 12 and in Figure 22, the damping rates of all but the first pole of the tapered nose model were substantially lowered. The lack of significant change in the damping rate of the first pole may have been the result of the offsetting effects of the resistive wires and the tapered nose.

TABLE 12. A COMPARISON OF THE RESULTS FROM PAST AND PRESENT MODELS

	Previous Model		Present Model	
Pole Number	Damping	Scaled Freq. (MHz)	Damping	Scaled Freq. (MHz)
First	-0.26	7.60	-0.27	7.51
Second	-0.34	13.10	-0.24	14.80
Third	-0.28	18.55	-0.18	18.56
Fourth	-0.28	24.40	-0.23	24.15
Fifth	-0.44	28.30	-0.35	30.72
Sixth	-0.34	35.60	-0.20	36.22
Seventh	-0.30	40.80	-0.16	40.01

The F-106B model used in this experiment was an approximate, not exact, model of the aircraft. By making detail changes on the model to make it more exact, the effect on the resonances of the fine detail could be determined. For example, the addition of a nose boom to the aircraft would make the model both longer and more exact, which should lower the frequency of the first pole. The frequency of the third and fourth poles might be raised by modifying the tail and the wings so that

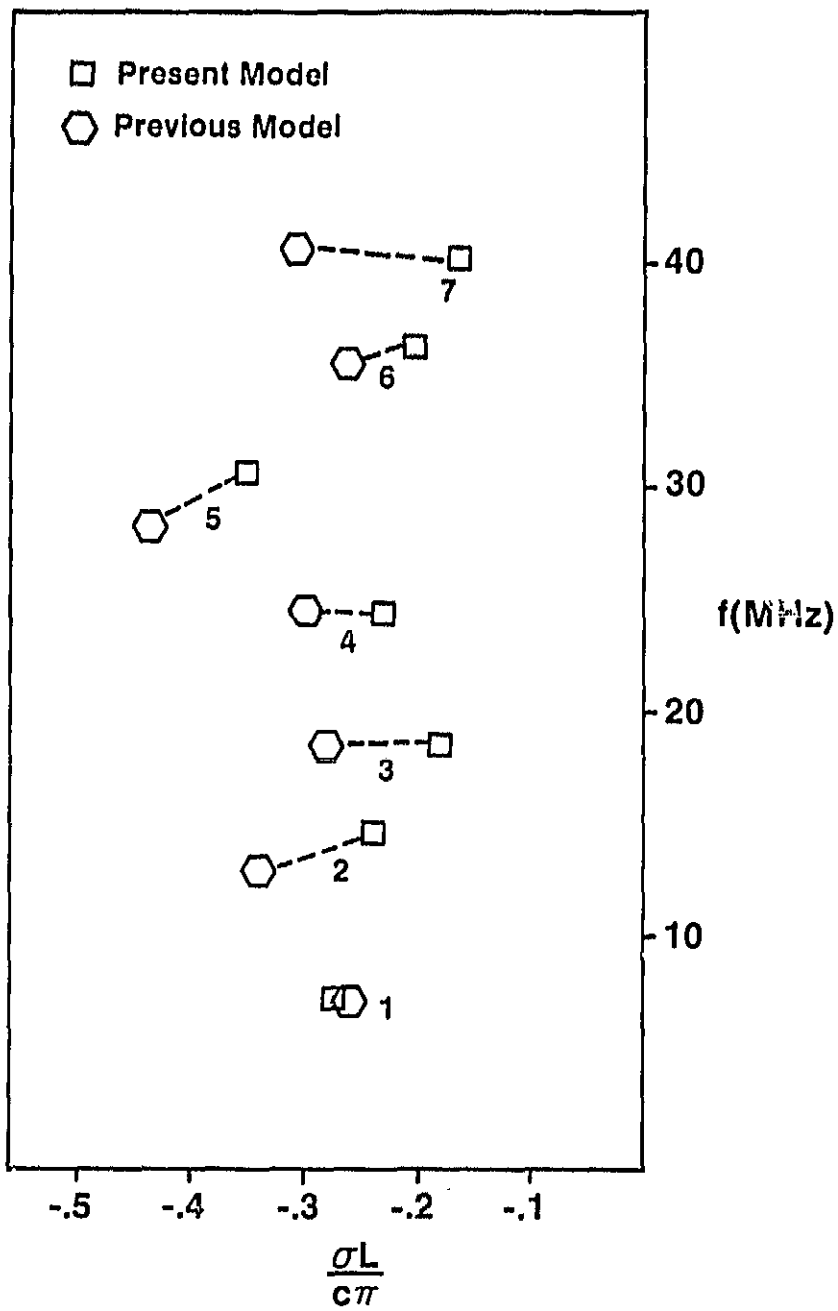

Figure 22. A comparison between the two different model results.

they would have a rudder and elevons like the real aircraft.

In both the B-dot and the D-dot waveforms there was a zero-frequency pole; i.e., the Prony program extracted a pole which represented an exponentially decaying term. In the B-dot waveform the zero-frequency pole was extremely stable, having a mean value of 0.05 and a variance of zero. In the D-dot waveform, however, the zero-frequency pole was rather unstable. The mean of its damping was 0.060, but it varied from 0.03 to 0.09 and had a standard deviation of 0.022. This zero-frequency pole is probably part of the pulse that was used to excite the model. On both of the cylinders, the Prony program also extracted zero-frequency poles in the D-dot and B-dot waveforms. In the cylinder results there were two zero-frequency poles rather than one.

V. CONCLUSIONS

Regarding the resonances of the cylinders, we can state the following results and conclusions:

1. The comparison between the large-diameter and small-diameter cylinders shows slightly stronger damping and lower frequencies for the large one (Fig. 9). Isolated cylinders would produce the same result.

2. The comparison between the present poles and those of Turner [Ref. 1] shows less damping in the present case (Fig. 10,11). This is expected since the smaller, more resistive wires in the present case result in less current conducted away from the cylinder.

3. The comparison with the poles of Yang [Ref. 6] shows reasonable agreement, and the comparison with Tesche [Ref. 5] shows the sort of difference expected: less damping in Tesche's case since his cylinders were isolated instead of wire-connected (Fig. 12). These comparisons give confidence in the basic correctness of our technique for determining poles.

From the F-106B model we have the following results and conclusions:

1. The comparison between the poles extracted from the B-dot sensor data and those from the D-dot sensor shows good agreement for most of the poles. More specifically, the agreement is good, within 10 percent, for poles 1, 2, 3, and 6; it is fair, 21 percent, for pole 4; but the data are insufficient for a good comparison on 5 and 7 (Fig. 20, Table 10). Ideally, the poles should agree exactly, so the discrepancies that are observed (which are usually less than 10%) give an idea of the accuracy of the poles of the model.

2. The comparison between the poles of the model and those of the actual airplane shows rough agreement, the damping of the first pole being responsible for the largest discrepancy (Fig. 21). Poles from only one lightning event on the airplane were used for this comparison [Ref. 7]. Other poles have been obtained from airplane data and may be seen plotted in Reference 1, but these poles are less reliable because of larger quantization errors and the lack of simultaneous B-dot and

D-dot waveforms for corroboration of the values.

One would like to have pole sets for both the model and the in-flight data in a situation where the attachment points were known to be the same. Then, differences in the pole sets could be interpreted as resulting from the lightning channel having an impedance either higher or lower than the wires. Thus, something would be learned about the channel and its effect on the resonances. Because the attachment points for the in-flight lightning event used here are not known, current conclusions cannot be too specific regarding the channel. However, rough agreement is being obtained with the use of the present wires, and some of the existing discrepancy may be due to attachment point location variations between the model and the in-flight situations.

One other possible source of discrepancies between the poles of the model and the airplane is the shape of the model: it is not an exact scale model of the airplane. Future work should perhaps be aimed at making the required detail improvements to the shape.

3. The comparison between the poles of the present model and those of Turner shows the effect of the change to resistive wires and a tapered nose. The damping of all the poles but the first has been reduced (Fig. 22). This is as expected and is the same effect seen in the case of the cylinders. On the model, this reduced damping improves the agreement with the in-flight results.

4. The distribution of the poles in the complex plane is different for the F-106B model than for the cylinders. Whereas the poles of each cylinder lie evenly along a line which slopes gently to the left (Fig. 10,11), the poles of the model are rather scattered and show a tendency to lie farther to the right at the higher frequencies (Fig. 21). This is also true of the in-flight poles (Fig. 21).

Some comments are in order regarding our experiences using Prony analysis on laboratory data, in-flight data, and computer generated data. For computer generated waveforms which consist of several damped sinusoids without noise or distortion, the Prony code works very well, extracting the correct values of all the poles, both damping and frequency, even when some of the residues are very weak compared to others.

In some cases, the frequencies of the poles can also be picked out by inspection of the Fourier spectrum of the waveform. However, in many cases the spectrum simply does not reveal the weak poles.

In the Prony analysis of waveforms which are measured rather than computer generated, there are two problems. First, the Prony code often will not fit the waveform. That is, the RMS error between the actual waveform and the one generated from the Prony poles and residues is larger than, e.g., 50 percent. This is a common occurrence in the analysis of in-flight waveforms. When it happens, the poles are not used. Second, in the case where there is a good fit (RMS error < 5%), a question exists as to whether the poles are really the true natural frequencies of the object under test, or whether they differ from these because of noise or distortion in the measured waveform. One example of distortion is the quantization error discussed in Reference 7, which was found to lead to incorrect damping rates for the poles.

To gain a degree of confidence in the natural frequencies, the practice has been to analyze simultaneous B-dot and D-dot waveforms and make a comparison of the resulting poles. If they agree closely, which often happens for the laboratory data, they are accepted as giving the true natural frequencies (including those of the input waveform).

One method tried on the model data when B-dot and D-dot poles differ, was to filter out some of the poles and then re-run the Prony code on the filtered waveform. This gives the code a simpler waveform to work with and, as described in Section IV, can lead to better agreement between B-dot and D-dot poles.

The Prony code appears better suited to measured waveforms, which have their pole frequencies well separated, than to those with closely spaced poles. For example, the pole extraction was less troublesome for the cylinder, where the sensor was located at the center so as to pick up only every other pole, than for the F-106B model with its many poles.

For some measurements, the correctness of the natural frequencies can be checked in another way--by comparison with theoretical calculations. This has been done in the case of the cylinders.

REFERENCES

[1] Turner, C. D., and T. F. Trost, "Laboratory Modeling and Analysis of Aircraft-Lightning Interactions," Report on NASA Grant NAG1-28, NASA CR 169455, August 1982.

[2] Kay, S. M. and S. L. Marple, Jr., "Spectrum Analysis - A Modern Perspective," Proc.IEEE, Vol. 69 (11), pp. 1380-1419, November 1977.

[3] Poggio, A. J., et al., "Evaluation of a Processing Technique for Transient Data," IEEE Transactions on Antennas and Propagation, AP-26, p. 165, January 1978.

[4] Van Blaricum, M. L. and R. Mittra, "Problems and Solutions Associated with Prony's Method for Processing Transient Data," IEEE Transactions on Antennas and Propagation, AP-26, p. 174, January 1978.

[5] Tesche, F. M., "On the Sigularity Expansion Method as Applied to Electromagnetic Scattering from Thin Wires," EMP Interaction Note 102, Air Force Weapons Laboratory, Kirtland AFB, New Mexico, 1972.

[6] Yang, F. C. and K. S. H. Lee, "Natural Frequencies of a Post Attached to a Lightning Return Stroke," Lightning Phenomenology Note 8, Air Force Weapons Laboratory, Kirtland AFB, New Mexico, 1983.

[7] Trost, T. F., C. D. Turner, and C.-T. Wen, "Some Results and Limitations of Prony Analysis of In-flight Lightning Data," 8th International Aerospace and Ground Conference on Lightning and Static Electricity, June 1983, DOT/FAA/CT-83/25, pp. 17-1 through 17-8.

[8] EG&G, Albuquerque, New Mexico, Data Sheet 1100, September 1980.

[9] EG&G, Albuquerque, New Mexico, Data Sheet 1118, September 1980.